PhD program in Molecular Medicine

Cycle: XXXI

A.Y. 2017/2018

PhD Thesis

The KCASH2^{KO} mice: a new mouse model with mild cerebellar Hedgehog-dependent phenotype and spermatozoa abnormalities

Candidate:

Mariapaola Izzo

PhD Program Coordinator:

Prof. Isabella Screpanti

Tutor:

Prof. Enrico De Smaele

TABLE OF CONTENT

INTRODUCTION

The Hedgehog signalling pathway

The Hedgehog (Hh) signalling pathway (**Fig.1**) plays a significant role in signal transmission from the cell membrane to the nucleus. Hh is crucial during normal invertebrates and vertebrate's embryonic development and it is involved in several processes including cell proliferation, differentiation as well as in adult tissues regeneration and homeostasis (Eguether and Hahne; 2018). Moreover, the Hh signalling results to be disrupted in several types of human cancer (Carballo G. et al., 2018; Teglund et al., 2010).

Nusslein-Volhard and Wieschaus discovered the Hedgehog gene in 1980 through genetic screening examining segmental development in the fruit fly *Drosophila melanogaster* (Nusslein-Volhard and Wieschaus, 1980). The Hh pathway is highly conserved from flies to humans and many of the core components are easily recognized as orthologs with the same function. In vertebrate three homologs of the Hh gene have been identified: Sonic Hedgehog (Shh), Indian Hedgehog (Ihh) and Desert Hedgehog (Dhh) (Wada H. et al, 2006).

Of the three family members, Ihh has been involved in endochondral bone formation, as a negative regulator of chondrocyte differentiation, and participates in the development of gastrointestinal tract and mammary glands (Vortkamp et al., 1996; van den Brink et al., 2004; Lewis et al., 2004). Dhh is the closest homologue of *Drosophila melanogaster* HH ligand. Its expression is mostly restricted to gonads, including Sertoli cells in the testis, where it plays a key role in the germ cells differentiation (Sahin et al., 2014; Zou et al., 2012).

Shh is the main activating ligand of the Hedgehog signalling pathway. In mammalian, Shh is expressed in several tissues, where it plays an essential role in embryonic development, regulation of cell differentiation, cell proliferation. In the central nervous system (CNS)

modulation of Shh is critical for cerebellar tissue polarity and cerebellar differentiation (Tadas K. Rimkus, 2016; Ruiz i Altaba et al., 2002).

Shh is a protein able to activate both an autocrine and paracrine signalling. It is synthesized as a 45 KDa precursor protein that undergo to an autoproteolytic cleavage by its own C-terminal domain into two secreted peptides: a 19 KDa amino terminus (Shh-N), with a signalization domain, and a 26 KDa carboxy terminus (Shh-C), lacking any known signal transduction activity. This cleavage allows the covalent attachment of a cholesterol moiety to their carboxyl terminus and a palmitate moiety to their amino terminus (Cohen MM Jr., 2004). These lipid modifications are necessary for the proper movement and reception of the ligand.

Most of the molecular events that trigger the activation of the Shh pathway take place in cells' primary cilium (Huangfu D. et al, 2005). The primary cilium is an organelle which extends from the maternal centriole to cell surface of most vertebrate cells and acts as sensor of chemical signals necessary for cell division. Growing cells have a primary cilium during S-phase, which is disassembled prior each cell division. In G2-M phase, cilium shortening occurs, leading to its eventual resorption or release from the plasma membrane. The primary cilium plays a critical role in transducing the Hh signalling (Carballo G. et al., 2018; Barakat et al., 2013; Lin et al., 2012) (**Fig.1**). Shh binds its specific receptor Patched1 (Ptch1), a 12-pass transmembrane proteins with two large extracellular loops and two large intracellular loops which is localized at the base of primary cilium (Albert F. et al, 2012). Within the extracellular loop structure, there is a sterol-sensing domain that is thought to interact with cholesterol bound to HH protein (Ingham et al., 2000). In absence of the ligand Shh, Ptch1 acts as an inhibitor of the pathway blocking the activation of the co-receptor Smoothened (SMO), a 7-motif receptor transmembrane belonging to the G protein-coupled receptors family (GPCRs), through its degradation or sequestration in an intracellular compartment

(Wu et al, 2012). In this context, the transcription factors of the pathway, named Glioma-Associated Oncogene Homolog 1 (Gli1), Gli2 and Gli3, are sequestered in the cytoplasm by Suppressor of Fused (SuFu), which negatively regulates the mammalian Shh pathway (Skoda et al., 2018). The interaction of Shh with Ptch1, results in the release of SMO inhibition. SMO is then phosphorylated by Casein kinase 1a (CK1a) and G-protein coupled receptor kinase 2 (GRK2). The phosphorylated SMO interacts with β-arrestin, facilitating SMO ciliary accumulation, and with anterior-grade trafficking motor kinesin-II (Kif3A) kinesin motor proteins, promoting the formation of a complex with the ciliary proteins EVC (Ellis-van Creveld syndrome protein) and EVC2, which supports the dissociation of the Sufu-Gli complex (Yang et al., 2012). Therefore, this downstream signalling cascade results in the translocation of Gli family proteins in to the nucleus and initiation of target genes transcription. The three mammalian Gli proteins share a similar DNA-binding domain comprising five-tandem C2H2 zinc-finger and a C-terminal activation domain but have different functions and post-translational modifications. While Gli1 occurs as a full-length transcriptional activator, Gli2 and Gli3 can act as either positive (Gli2-A and Gli3-A, the full-length proteins) or negative (Gli2-R and Gli3-R, the cleaved repressor forms) regulators of the pathway (Ruiz I Altaba et al., 1997; Pan et al., 2006). Gli1 is a strong constitutive transcriptional activator and also a Gli transcriptional target, which enhances its own expression, thus auto-reinforcing the signalling strength. Other Gli transcriptional targets genes are components of the Hh signalling, such as the Hh interacting protein (Hip), Ptch1, Bone Morphogenetic Proteins (BMPs) (Wu et al, 2012).

Shh signalling controls proliferation, patterning and/or migration, and survival of a number of cell types, including retinal precursor cells, myoblasts, optic nerve, astrocytes, cerebellar granule cells (Dahmane et al., 1999), and neural progenitor cells (NPCs), regulating cell cycle genes (e.g. cyclin D1, cyclin D2 and N-Myc), the antiapoptotic protein Bcl-2 (Cayuso

et al., 2006), insulin-like growth factor 2 (IGF2), platelet derived growth factor receptor-α (PDGFR-α), c-myc, Bmi1, Wnt and Hes1 (**Fig.1**).

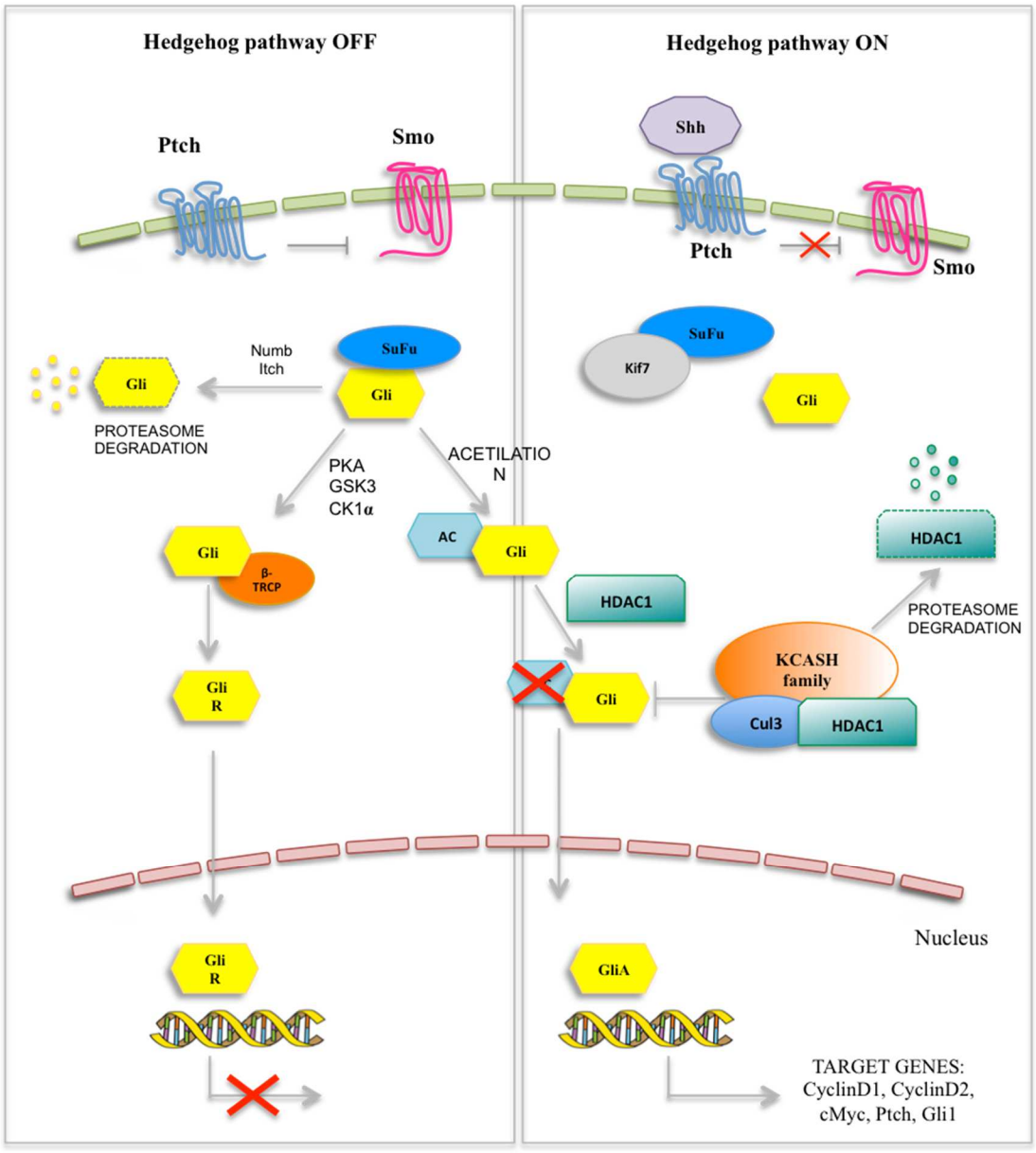

Fig.1The Hedgehog signaling pathway.

In the absence of Hh ligand, suppressor of fused (SuFu) forms a complex with the Gli transcription factors. Different mechanism regulates fine-tune the Gli activity. Ligand binding to Ptch (ON) promotes the entry of the activating receptor Smo. This process allows the migration of active Gli into the nucleus where transcription of Hh target genes is activated.

The different cellular responses to Shh in several tissues during development reflect the presence of a complex mechanisms that dynamically regulate the Hh signalling.

Several mechanism regulating Gli proteins activity have been identified: phosphorylation, proteolysis, acetylation, which, restricting signal duration and inhibiting this process, can lead to disruption of cell patterning or excessive cell proliferation (**Fig.1**).

For example, in the unstimulated state, a set of kinases including protein kinase A (PKA), glycogen synthase kinase 3β (GSK3) and casein kinase I (CKI) regulate the state of Gli phosphorylation. These kinases phosphorylate multiple sites in the C-terminal region of Gli proteins (mainly Gli2 and above all Gli3) and causes the recruitment of Slimb/β-TRCP. This recruitment leads to proteolytic cleavage of Gli full length into C-terminally truncated repressor form, Gli-R. Gli-R moves into the nucleus where it binds to Shh target gene repressing their expression. The kinesin protein KIF7 is another Shh signalling regulator. In response to Hh activation, KIF7 localizes at the base of the primary cilium, control the cilium structure, organize a specialized compartment necessary for Shh signalling and interact with Gli protein preventing Gli2 and Gli3 accumulation within the cilium (Jiang 2006, Smelkinston et al., 2007). The KIF7 dephosphorylation, mediated by protein phosphatase 2A (PP2A), facilitates KIF7 localization to the tips of primary cilium and promotes Gli transcriptional activity (Liu et al., 2014).

Gli1 and Gli2 acetylation represents an inhibitory signal, and their HDAC1-mediated deacetylation represents a transcriptional switch which promotes transcriptional activation and sustains a positive autoregulatory loop through Hh-induced upregulation of HDAC1 (Canettieri et al., 2010; Gulino et al., 2012; Coni et al., 2013) (**Fig.1**).

In addition, SuFu controls transcription by Gli factors. In fact, the association of SuFu with Gli3 promotes the conversion of Gli3 into the repressor form (Gli3R), which binds the promoter, but inhibits transcription of Shh target genes (Infante et al., 2018).

Finally, ubiquitination is a post-translational modification, which controls the localization, stability and activity of the key Shh signalling components, such as Ptch, Smo, SuFu and Gli (Di Marcotullio et al., 2007). Ubiquitination involves the linkage between the C-terminal glycine (Gly76) of the 76-amino acid protein Ubiquitin (Ub) and the ε-amino group of the lysine residues on the substrate (Popovic et al., 2014; Berndsen et al., 2014) (**Fig.1**). Ubiquitination is initiated by formation of an ATP-dependent covalent bond between the Ub molecule and the ubiquitin-activating enzyme (E1), which activates Ub and transfers it onto ubiquitin-conjugating enzyme (E2). Finally, an E3 ubiquitin ligase is responsible for the transfer of the activated ubiquitin molecules to the lysine of the target proteins.

Ubiquitinated proteins may be dedicated to different fates depending on the length or linkage of the ubiquitin molecules. For example, ubiquitination of Ptch and Smo may change their subcellular localization (Huang et al., 2013). Ptch ubiquitination by the E3 ligase Smurf may also lead to its degradation. In fact, Huang et al. discovered that this mechanism is required during endocytosis and subsequent Ptch protein turnover, responding to activators of the Hh signalling pathway (Huang et al., 2013).

Ubiquitination may play a role also in modulation of Gli family members. Di Marcotullio et al., found that the adaptor protein Numb targets Gli1 for ubiquitination and proteolytic degradation mediated by the HECT E3 ligase Itch (Di Marcotullio et al., 2011) (**Fig.1**). Gilder et al. showed that the adaptor protein Fem1b mediates Gli1 interaction with E3 ligase complexes containing Cul2/Elongin-BC and the consequent suppression of Gli1 dependent transcriptional activity (Gilder et al., 2013).

The Shh signalling pathway in cerebellar development

Shh is a pleiotropic factor in central nervous system (CNS) development, particularly it orchestrates many aspects of cerebellar development and maturation, and its misregulation can leads to Medulloblastoma, the most common paediatric malignant cerebellar tumour (Álvarez-Buylla A, Ihrie RA, 2014).

The CNS is composed by the brain and the spinal cord. The brain is divided into three major components: the brainstem, the cerebrum and the cerebellum. The cerebellum is a morphologically unique brain structure, composed by an elaborate set of folia separated by fissures; although it represents only the 10% of the total brain volume, it bears more than half of the neurons total amount. Cerebellum operates as a coordination centre, controlling smooth and skilful movements using sensory inputs reported from periphery. It is also involved in cognitive functions, including feed-forward sensory-motor learning and spatial memory (Lackey et al., 2018).

All mammals' mature cerebella have similar basic pattern of ten folia in the media Cerebella (vermis), suggesting that the foliation is highly conserved between species and tightly is genetically determined. The cortex of each folium consists of different well-defined neuronal cell populations, which are positioned in three district layers depending on its developmental state (proliferative, differentiative or migrating) (**Fig.2**). These layers consist of a molecular layer (ML), which is principally populated by granule cells axons and Purkinje cells' dendrites; the Purkinje cell monolayer (PCL) consisting of Purkinje cells' body, and the internal granule layer (IGL), consisting primarily of mature granule cell neurons (**Fig.2**).

Cerebellar growth and foliation are a distinct process in cerebellar morphogenesis which begin during early embryonic stage and persist up to one year after birth in human, whereas in mouse up to postnatal day 21 (P21), (Behesti H, Marino S et al., 2009).

The nervous system develops when the notochord induces its overlying ectoderm to become neuroectoderm and to develop into the neural plate. The neural plate folds along its central axis to form a neural groove lined on each side by a neural fold. The two neural folds fuse together and pinch off to become the neural tube. Neural folds fusion begins in the middle of the embryo and moves cranially and caudally. The tube's cranial open end is the anterior (rostral) neuropore, and the caudal open end is the posterior (caudal) neuropore. After its closure, the rostral part of the neural tube corresponding to the future brain, rapidly develops and undergoes dilations, constrictions and flexures resulting in the formation of 3 primary brain vesicles: the prosencephalon (forebrain), the mesencephalon (midbrain) and the rhombencephalon (hindbrain). The primary brain vesicles give rise to five secondary brain vesicles: Telencephalon, Diencephalon, Mesencephalon, Metencephalon and Myelencephalon which give rise to several adult structures. In particular, the Isthmic Organizer (IO), located at the junction of the Mesencephalon and the Metencephalon, gives rise to cerebellum (Butts T, Green MJ, Wingate RJ, 2014). The histogenesis of the cerebellum develops in 4 significant steps:

- Characterization of the cerebellar territory
- Formation of two distinct progenitor zones
- Migration of Cerebellar Neurons
- Differentiation of the Cerebellar Neurons and Formation of the Cerebellar Circuitry

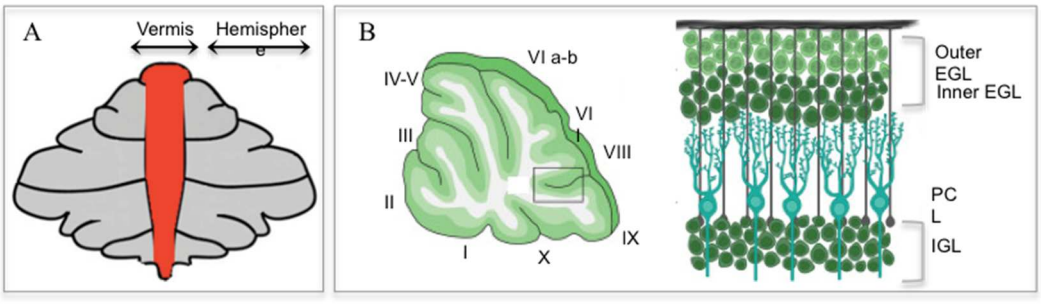

Fig.2 Cerebellum morphology.

(A) Image of mouse cerebellum. Mammalian cerebellum is divided into two later hemispheres. Lobules of the hemispheres are continuous with lobules in vermis. (B) Scheme for naming the lobules in the vermis with roman numerals I-X from anterior to posterior. A representation of the mouse cerebellar cortex. The outer EGL, inner EGL, Purkinje cell layer (PCL), and inner granule layer are show (IGL).

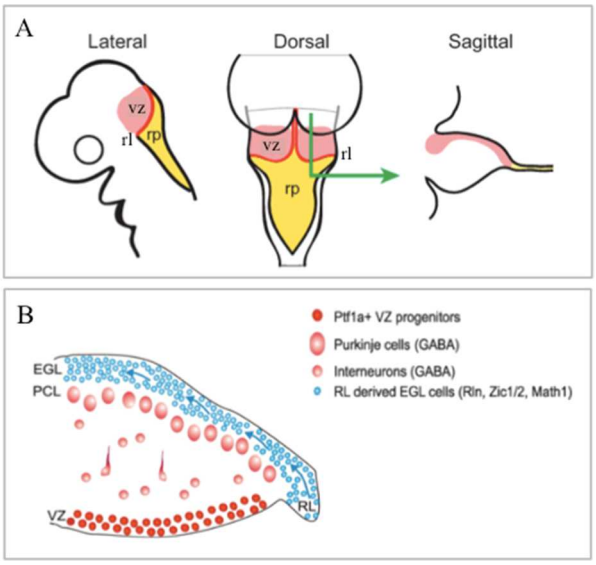

Fig.3 The histogenesis of the cerebellum.

(A) Anlage of the cerebellum showing the relationship between rhombic lip (rl), ventricular zone (vz), and roof plate (rp) of the fourth ventricle. (B)Schematic illustration of a coronal section of the midbrain-cerebellum-medulla region. Ptf1 expressing VZ progenitors produce GABAergic cells in the cerebellum, including PCs and interneurons. In parallel, RL progenitors produce granular cell precursors located in the EGL expressing Math1.

In mouse, approximately at embryonic day 8.5 (E8.5), the Isthmic Organizer region orchestrates the development of cerebellar and mesencephalic structures through the morphogenic activity of secreted factors, FGF8 (fibroblast growth factor 8) (Zhang XM. et al, 200). FGF8 is involved in the regulation of several genes expressed in the mid- and hindbrain regions (Wang and Zoghbi, 2001).

Following territorial specification, at E9 starts the cerebellar histogenesis. During this age the cerebellar anlage is formed from two separated and symmetric bulges which, during the following days, grow and fuse together, giving rise to the unitary cerebellar plate, comprising the vermis and the two hemispheres (De Luca A. et al., 2016). Such developmental phase is also characterized by the two germinative compartments formation, just above the opening of the fourth ventricle: the rhombic lip (RL), located at the outer aspect of the cerebellar plate, adjacent to the roof-plate, and the ventricular zone (VZ), placed in the inner side, covering the fourth ventricle (**Fig.3**). These germinative districts are defined by the region-specific expression of two basic helix-loop-helix transcription factors: the pancreas transcription factor 1-a (Ptf1-a), expressed in the VZ, and the mouse homolog of Drosophila atonal (Atoh-1), present in the RL (Hoshino M. et al, 2005). This spatially-restricted expression pattern defines the neurochemical compartmentalization of cerebellar precursors, as all GABAergic neurons (Purkinje cells, PCs, nucleo-olivary projection neurons of deep cerebellar nuclei, DCN, and all inhibitory interneurons - basket, stellate, Golgi and Lugaro cells) originate from Ptf1-a+ precursors (Seto Y. et al, 2014), while glutamatergic lineages (large projection neurons of DCN, unipolar brush cells, UBCs, and granule cells) derive from Atoh-1+ progenitors (Yamada M. et al, 2014).

The two primary germinative epithelia disappear at birth. During VZ division, precursors emigrate into the cerebellar prospective white matter (PWM), whereas those of the RL move along the pial cerebellar surface, where they form the external granular layer (EGL).

Proliferation of both roof-plate and ventricular-derived cells is sensitive to Shh signalling (**Fig.4**). In the roof plate, endogenous Shh production stimulates secondary proliferation from non-neural precursors adjacent to the rhombic lip (Huang et al., 2009).

Shh, secreted by Purkinje cells into the cerebrospinal fluid, acts to drive early ventricular zone proliferation. Later on, Shh has an effect on a population of secondary precursors of inhibitory neurons and on the Glia, which reside in the prospective white matter (Huang et al., 2010; Fleming et al., 2013). Finally, Shh signalling contributes to determination of the shape and size and number of cerebellar folia and modulates proliferation of cerebellar granule cells precursors in the EGL (De Luca A. et al, 2016) (**Fig.4**).

By the end of the third postnatal week, the cerebellum shape has been transformed from its embryonic flat, oval form to a more complex structure with deep fissure and large folia (Sudarov A and Joyner AL; 2007; Leguè E. et al., 2016).

Shh actively regulates the amplification of cerebellar progenitors in both embryonic and postnatal germinal zones. This morphogen, secreted by Purkinje cells from E17.5 (Lewis PM. et al, 2004) and by choroid plexi at earlier time points (Huang X. et al, 2010), controls the production of appropriate numbers of excitatory and inhibitory interneurons. In addition, it modulates the correct generation and development of Glial progenitors and it exerts specific functions in different phases of granule cell development, in both normal and pathological conditions, such as Medulloblastoma. Finally, Shh actively orchestrates the major dynamics of cerebellar foliation, sustaining normal processes of cerebellar growth and maturation (De Luca A. et al, 2016). In particular, proliferating GCPs, start to migrate out to the rhombic lip at E13, and spread over the roof of the cerebellar anlage to populate the outer EGL. At this point, GCPs are still expressing *Math1* and *nestin*, which labels undifferentiated precursors (Butts T, Green MJ, Wingate RJ, 2014).

After an initial burst of cell proliferation, the GCPs start a differentiation program by exiting the cell cycle and moving into the inner EGL. The GCPs proliferate actively for a long time, in mouse until the third week of postnatal life, and the peak of proliferation occurs close to the date of birth (Dahmane and Ruiz i Altaba, 1999; Lewis et al., 2004).

The next stage of GCPs development is the inward migration along the processes of Bergman Glial fibers to their definitive deeper site, the internal granule layer (IGL), where differentiated granule neurons reside. In the IGL, these cells are expressing mature markers such as tag1 (tubulin-associated glycoprotein 1) and Class 3 β-tubulin (Dahmane and Ruiz i Altaba, 1999; Wechsler-Reya and Scott, 1999; Wallace, 1999; Lewis et al., 2004). It has been demonstrated that at this stage they are actively controlled by mitogenic factor secreted by Purkinje cells.

The Purkinje cells release Shh to control the proliferation of granule precursor cells (GCPs) but aberrant levels of Shh activity lead to a wide spectrum of disease ranging from neurodevelopmental defect to cancer and Shh activity is switched off by different mechanisms. The canonical Shh pathway switch off occurs regulating the Gli activity.

As previously described, the inhibition of Gli activity by Shh operates at multiple levels. Shh promotes cytosolic over nuclear localization of Gli2, induces Gli2 and Gli3 processing into repressor forms, and activates cAMP-responsive element binding protein that in turn represses Gli1 transcription (Belgacem and Borodinsky, 2015). Failure to interrupt Shh signals results in uncoordinated proliferation and differentiation of GCPs and eventually leads to malignancy (**Fig.5**). Shh pathway activation may be due to alteration of Hh components such as Patched, Gli1 and Gli2. Alteration of the Shh pathway have been linked to several developmental pathologies and tumorigenesis. In fact, mutations in Patched gene, which activate the Shh pathway, have been described in Basal Cell Nevus Syndrome

(Gorlin), associated with developmental pathology and tumours as the Dandy-

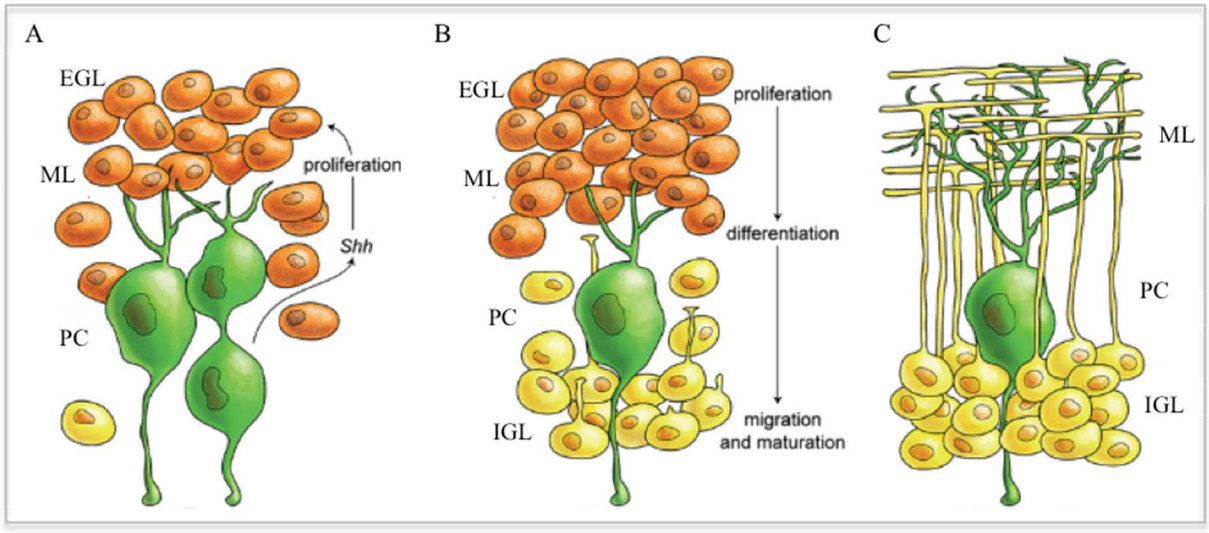

Fig.4 Germinal zones in the developing cerebellum.

Cerebellar cortex at around P4 (A), at around P10 (B), and in adult (C) is shown. Purkinje cells (green) express Shh that increase proliferative activity of external granule layer cells (EGL). Granule cells differentiate and migrate cross Purkinje cells layer to final destination in internal granule layer (IGL). PC: Purkinje cells; ML: molecular layer; EGL: external granule layer; IGL: internal granule layer.

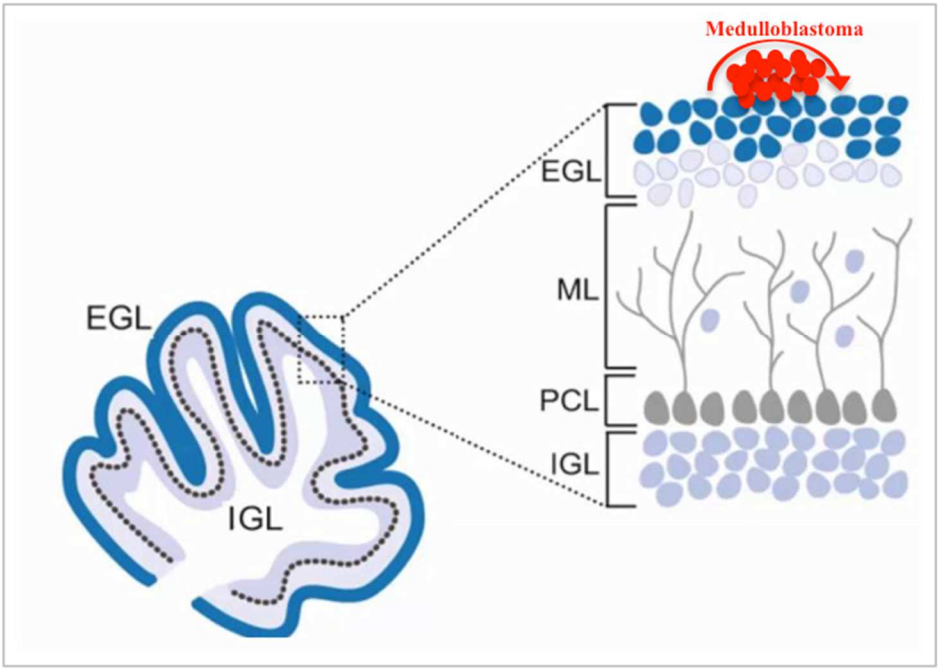

Fig.5 Deregulated Shh signaling in GCPs causes Medulloblastoma.

Granule cells progenitors in EGL normally turn off the Shh signaling pathway to differentiate and migrate to the IGL. Where the Shh pathway remains active, granule cells precursors keep proliferating and may give origin to MB.

Walker syndrome, the Joubert syndrome, cerebellar hypoplasia, as well as, one of the most malignant paediatric brain tumour called Medulloblastoma (**Fig.5**).

Deregulation of the Hedgehog signalling pathway: The Medulloblastoma

Medulloblastoma (MB) is a malignant embryonal tumour of the cerebellum, it accounts for 20% of malignant childhood brain tumours and this tumours mainly occur during infancy and childhood, but a small percentage occur in adulthood (Yi et Wu, 2017). The fourth edition of the World Health Organization (WHO) classification of tumours of the central nervous system, published in 2007, classifies the different types of MB depending on their histological features (**Fig.6)**. MB is divided in five categories: classic, desmoplastic or nodular, Medulloblastoma with extensive nodularity, anaplastic and large cell Medulloblastoma (Gilbertson and Ellison, 2008). However, it has become evident that histological classification was not sufficient. Transcriptional profiling studies, derived from microarray data of large numbers of patients with MB, have highlighted the existence of four different subgroups of MB depending on their demographics, transcriptomes, somatic genetic events, and clinical outcomes: WNT, Shh, Group 3 and Group 4 (Taylor at al., 2012). These advances in the field of Medulloblastoma classification, in addition to the histological features, are indispensable to stratify patients and provide adapter treatments. Finally, using a combination of molecular profiling and histology, the World Health Organization (WHO) currently divides MB into five subtypes (Louis et al., 2016): WNT-activated with classic histology; SHH-activated (wild-type TP53), with classic, desmoplastic/nodular, or large-cell/anaplastic histology; SHH-activated (mutant TP53), with classic or large-cell/anaplastic histology; non-WNT/non-SHH, group 3, with classic or large-cell anaplastic histology; non-WNT/non-SHH, group 4, with mostly classic histology (**Fig.6)**.

The Shh signalling pathway plays an important role in the embryonic development of the cerebellum, and consequently, its role in the MB formation is not surprising. Shh subgroup has an intermediate prognosis with a 5-year overall rate of 75%. It presents 30% of MB cases. It occurs mostly in infant and adults, being less common in children. It occurs more in male than females. This subgroup appears to be uncommonly metastatic (Bihannic and Ayrault, 2015).

The formation of MB occurs when the Shh pathway is constitutively activated in GCPs and the proliferation continues outside the normal developmental period.

Genomic alteration in components of the Shh signalling pathway have been identified in more than one-third of sporadic human MB cases and are associated with aberrant activation of Shh pathway that is either linked to PTCH mutation or PTCH locus chromosomal loss (45% of cases) and inactivating mutation of SuFu and/or activating mutation of SMO (Hallahan et al., 2004; Oliver et al., 2005; Guerrini-Rousseau et al., 2017). Mutation in PTCH was first found in the inherited Gorlin's syndrome, a disease in which patients develop numerous basal cell carcinomas and are predisposed to MB (Manoranjan et al., 2012). While SMO mutation are more frequent in adults, mutations of SuFu are mostly found in paediatric patients (0-3 years) (Guerrini-Rousseau et al., 2017). Recently, has been demonstrated that many mutations occur in the C-terminal region of SuFu thus affecting the K321 and K475 residues, suggesting that alterations in Itch-mediated SuFu ubiquitylation might play a key role in MB development (Infante et al., 2018).

Karyotype analysis of MB specimens has revealed isochromosome 17q as the most common cytogenetic abnormality. This chromosomal anomaly is the result of the chromosome short arm (p) loss, and subsequent "head to head" apposition of the long arms (Cogen and McDonald, 1996).

In MB, deletion of the chromosome 17p occurs in up to 50% of the karyotypes examined and it has also been shown to have implications in clinical management, as the loss of DNA sequences located on this chromosome arm is strongly associated with a negative prognosis for these patients (De Smaele et al., 2004). On this chromosome are located several tumour suppressor genes, such as p53, Hic, Mnt (Myc inhibitor) and REN-KCTD11 (KCASH1).

REN-KCTD11 gene maps on chromosome 17p13.2 and its deletion was found in 39% of the sporadic MBs (Di Marcotullio et al., 2004; Argenti et al., 2005). It has been identified as a negative regulator of Shh-dependent events, thus antagonizing both Shh-induced growth and block of differentiation of GCPs cultures, by affecting Gli1 nuclear transfer. REN-KCTD11 promotes neural cell growth arrest and $p27^{kip1}$ expression, and its abrogation in embryonic stem cells prevent the retinoic acid-induced upregulation of the proneural basic helix-loop-helix transcription factors neurogenin1 and NeuroD, which promote differentiation of inner EGL GCPs (Di Marcotullio et al., 2004; Argenti et al., 2005). The loss of such an inhibitory signal might therefore lead to the Shh-dependent uncontrolled GCP overgrowth linked to MB development. REN-KCTD11 loss of function is observed in all 17p deleted medulloblastomas (Di Marcotullio et al., 2004; De Smaele et al., 2004).

Therefore, 17p deletion might lead to the loss of Shh inhibitor mechanism by integrating multiple haploinsufficient conditions until they reach the threshold necessary to unmask cooperation with the Hedgehog master oncogenic pathway (De Smaele et al., 2004; Ferretti et al., 2005).

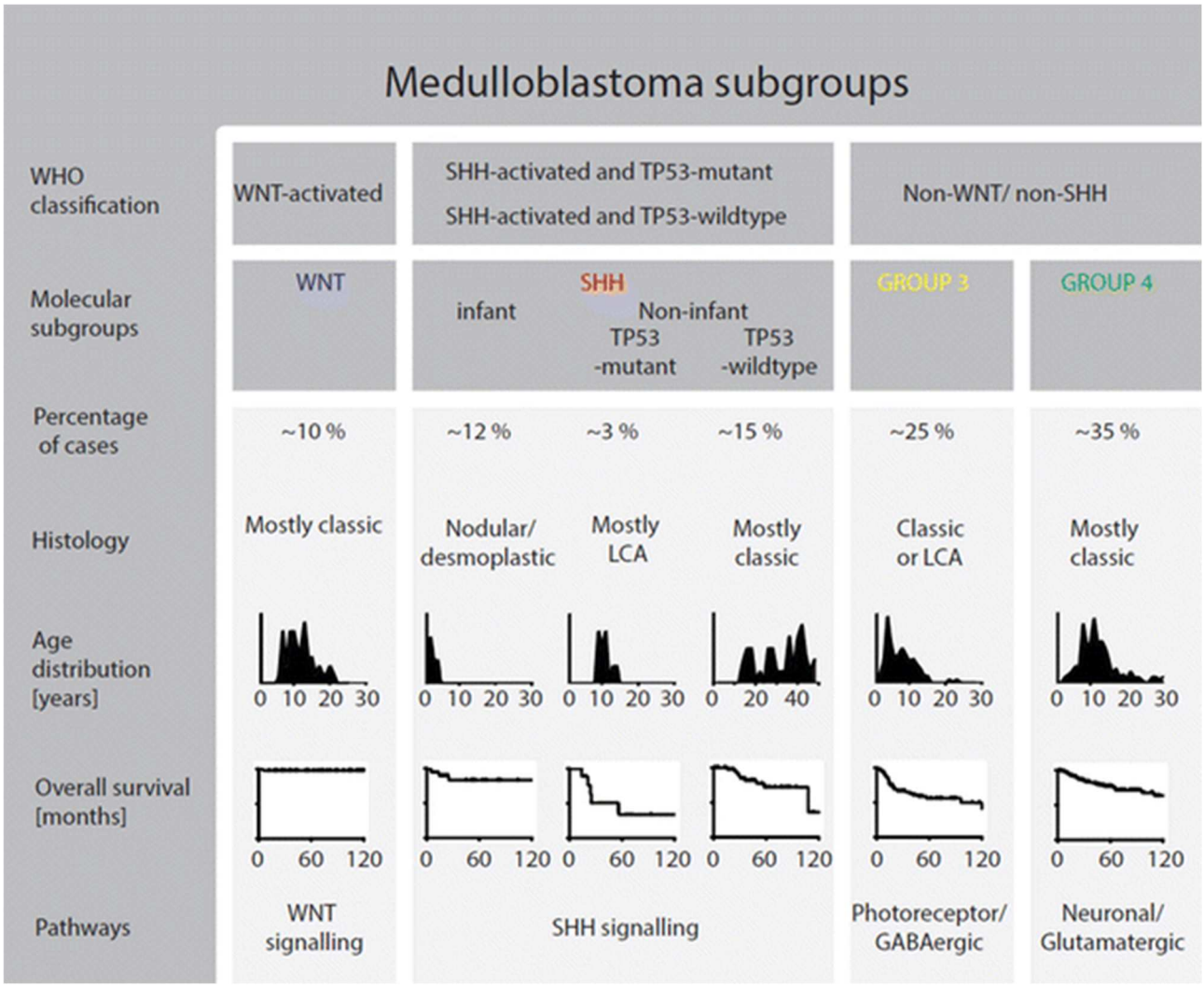

Fig.6 Molecular Subgroups of Medulloblastoma.

Comparison of the various subgroups of Medulloblastoma (from Neumann et al.,2017).

The KCASH family of protein

The search for REN-KCTD11 protein homologues in the public database and the subsequent analysis on the Ensemble genome browser resulted in the identification of two Open Reading Frame (ORF) coding for potassium channel tetramerization domain containing 21 (KCTD21) and potassium channel tetramerization domain containing 6 (KCTD6) putative proteins (De Smaele et al., 2011). Alike REN-KCTD11, also KCTD21 and KCTD6 are expressed in adult human brain and cerebellum; they have high similar amino acids sequence (42% and 32% with KCTD11 respectively) and strong BTB domain homology (58% and 54% with KCTD11 BTB respectively) (De Smaele et al., 2011) (**Fig.7**, panel A).

These homologies within the three KCTD-containing proteins suggest that they belong to a family of gene which shares common structural and functional features and may play similar biologic roles. For this reason, recently has been identified and characterized the new family of proteins named KCASH, as "KCTD containing, Cullin3 adaptor, suppressor of Hedgehog" (De Smaele et al., 2011) (**Fig.7,** panel A).

The KCASH family of proteins consists of three members: KCASH1 (REN-KCTD11), KCASH2 (KCTD21) and KCASH3 (KCTD6), and it is a subfamily of Potassium (K^+) Channel Tetramerization Domain-containing (KCTD) protein which is involved in fundamental physio-pathological process (Liu et al., 2013). Indeed, KCTD members are involved in a variety of diverse biological function processes which include among the others, protein ubiquitination and degradation (Correale et al., 2011; Canettieri et al., 2010; De Smaele et al., 2011), human genetic disease risk, including Medulloblastoma (Mancarelli et al., 2010), breast carcinoma (Faryna et al., 2012), obesity (Yoganathan et al., 2012), and pulmonary inflammation (Koehler et al., 2004). The 25 members of the family share a common N-terminal Bric-a-brack, Tram-track, Broad complex (BTB) domain (also known

as the POZ domain) (Liu et al., 2013). The BTB domain is a highly conserved motif (from *Saccharomyces Cerevisiae* to *Mammalian*) of about 100 amino acids, is a versatile protein-protein interaction motif that facilitates homodimerization or heterodimerization, as well as multimerization. Many functions have been identified for the BTB domain-containing KCTD proteins. These functions include transcriptional repression, cytoskeleton regulation, tetramerization and gating of ion channels and interaction with the Cullin E3 (Cul3) ubiquitin ligase complex (Liu et al., 2013; Smaldone et al., 2016). A variety of functional role of KCTD proteins have been identified in several signal pathways, including Sonic hedgehog (Shh) (De Smaele et al., 2011; Canettieri et al., 2010; De Smaele et al., 2004), Wnt/beta-catenin, FGF, and GABA signalling (Schwenk et al., 2010; Seddik et al., 2012).

KCASH1 is a tumour suppressor, involved in cerebellum granule differentiation. KCASH1, frequently deleted in human Medulloblastoma, is expressed in proliferating neuroblasts of the embryo cortical ventricular zone and induces growth arrest and differentiation of neural progenitors, in particular in GCPs during the transition from outer to inner EGL and in IGL cells of the developing cerebellum (Gallo et al., 2002; Argenti et al., 2005). Furthermore, this protein was identified as a part of Cullin E3 ubiquitin ligase complex, participating in the mechanism of deacetylation and activation of Gli1 and subsequently suppressing Hedgehog signalling. KCASH1, forming with Cullin3 an E3 ubiquitin ligase complex, inhibits HDAC1, blocking deacetylation of the transcription factor Gli1 and inhibiting its transcriptional activity (Canettieri et al., 2010) (**Fig.7,** panel B).

The other two components of the KCASH family of proteins shares common structural and functional features and acts in concert to suppress the Shh signalling. In fact, through their BTB domain, KCASH proteins are able to form homodimers and heterodimers with each other, with the exception of KCASH2-KCASH3 (De Smaele et al.,2011), and to bind Cullin3 E3 ubiquitin ligase, leading to HDAC1 ubiquitination and degradation (De Smaele et

al.,2011). Although all the three members of the KCASH family mediate the HDAC1 suppression, only KCASH3 is not able to directly bind HDAC1, but acts in form of heterodimer with KCASH1. This feature suggests the presence of two functionally distinct classes of KCASH proteins: the first composed by KCASH1 and KCASH2, which is active directly on HDAC1 also as homodimers; and a second class composed of KCASH3, which cannot bind directly HDAC1 but required heterodimerization with KCASH1.

Genetic and epigenetic events, that can reduce the KCASH family members expression, cause the accumulation of HDAC1, that may lead to Hh-dependent MB growth, as a result of persistent Gli1 deacetylation.

Human KCASH2 is located on chromosome 11q14.1. Interestingly, chromosome 11q is lost in several tumours including MB (Reardon et al. 2000). Allelic loss of KCASH1 and KCASH2 has been demonstrated experimentally by our research group in 35% (KCASH1) and in 10% (KCASH2) of a group of MB samples (Di Marcotullio et al, 2004; De Smaele et al., 2011), suggesting that genetic loss of these genes is a relevant mechanism in MB formation. Interestingly, even though none of the MB analysed presented deletion of both KCASH1 and KCASH2, all tumours analysed presented a reduced expression of both genes (De Smaele et al., 2011).

Interestingly, in silico analysis has highlighted that KCASH2 expression is reduced not only in HH-dependent MB, but also in other tumour types which are currently described as non-HH-dependent. Furthermore, our observations suggest that also several non-Hh MB exhibit an overall reduction of KCASH2 expression (De Smaele et al., 2011). Finally, loss of chromosome 11q has been observed in leukaemia (Stankovic et al., 2014) and prostate cancer (Schleutker et al., 2003). These observations suggest that KCASH2 may modulate additional pathways or processes involved in tumorigenesis.

First of all, loss of KCASH may induce HDAC increased stability in other physiological and pathological processes. In fact, the regulation of gene expression through histone deacetylation is an important mechanism not only in CNS development. Indeed, HDAC1 is found overexpressed in prostate and gastric cancers, where it indicates a poor prognosis, as well as in lung, oesophageal, colon and breast cancers (Halkidou K. et al., 2004; Choi JH. et al., 2001; Zhang Z. et al., 2005).

Furthermore, the KCASH2 may play other physiological functions not yet discovered, which may be relevant in other biological and pathological processes.

For this reason, it is essential to study in vivo the physiological relevance of KCASH2 through the generation of a new mouse model. This model could represent a novel model of Hh signalling alteration, to compare to other models already characterized.

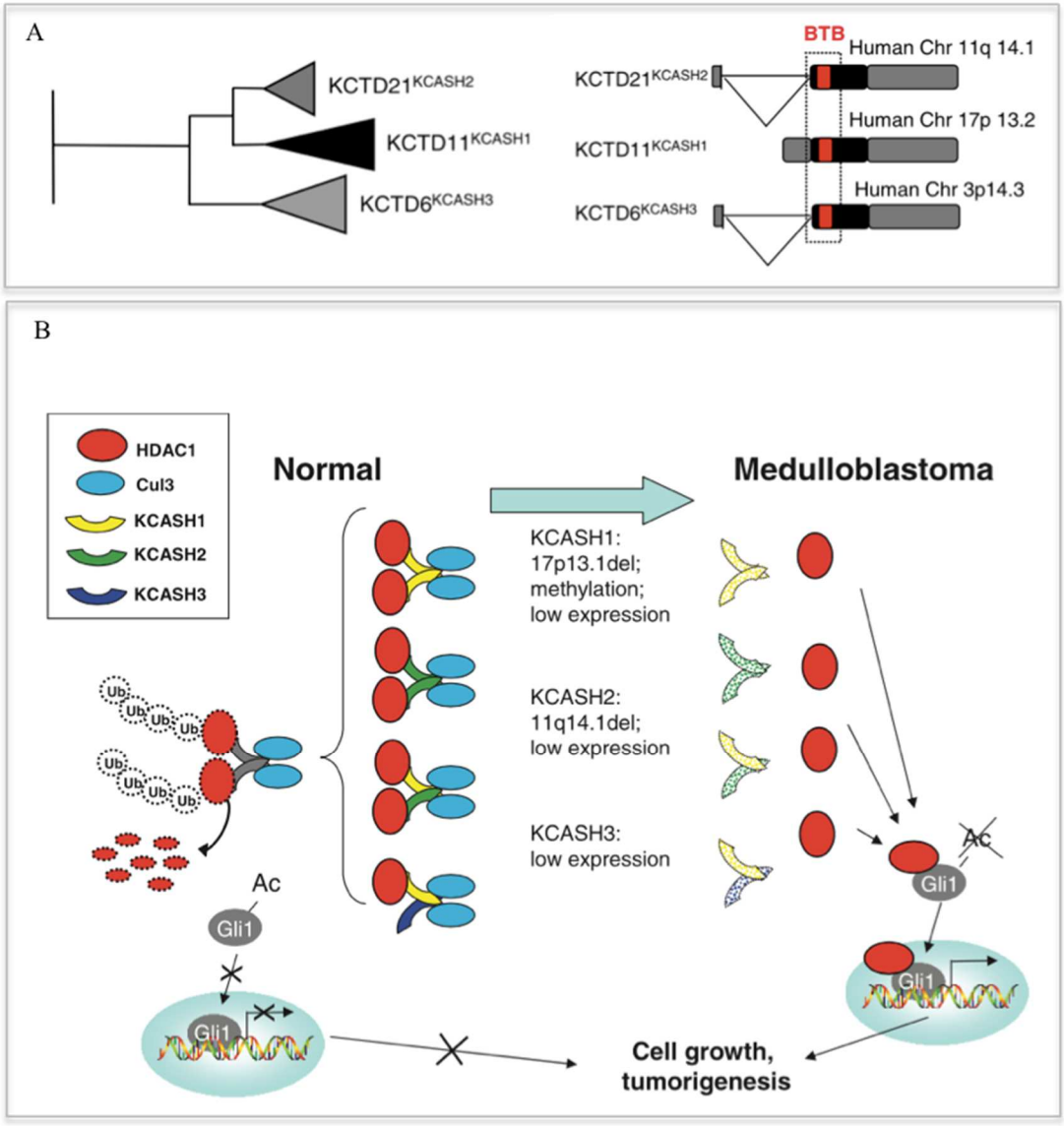

Fig.7 KCASH members and their role in regulation of Hh pathway.

(A) Representation of the KCASH family and structural domains of KCASH proteins. (B) Representation of the KCASH mechanism of action (De Smaele et al., 2011).

Mouse models for the study of Hedgehog pathway

The genetically engineered mouse model (GEMMs) has been an essential tool for uncovering the molecular and cellular basis of human diseases, including cancer. The GEMMs is useful to better understand genes functions and molecular mechanism behind cancer biology, as well as in translational cancer research, as preclinical models, to test targeted therapies; but also, to elucidate unknown physiological mechanisms, as the regulation of cerebellar foliation. The different mouse modelling technologies described above have been applied to studies of MB biology, genetics and preclinical research. Table 1 summarizes many of the genetically engineered MB mouse model currently published in the literature (Wu et al., 2011).

Table 1. Medulloblastoma genetically engineered mouse models (GEMMs)

Genotype	MB profile	MB incidence	Tumor latency (weeks)	Leptomeningeal metastasis	Reference
$Ptc^{+/-}$	Shh/desmoplastic	14%	5–25	No	15
$Ptc^{+/-}$ $P53^{-/-}$	Shh/desmoplastic	95%	4–12	No	18
$Ptc^{+/-}$ $Ink4c^{-/- \text{ or } +/-}$	Shh/desmoplastic	30%	12–36	No	19
$Ptc^{+/-}$ $Kip1^{-/- \text{ or } +/-}$	Shh/desmoplastic	60%–70%	16–18	No	20
$Ptc^{+/-}Hic1^{-/-}$	Shh/desmoplastic	~40%	by 25	No	22
$Math1\text{-}Cre/Ptc^{C/C}$	Shh/desmoplastic	100%	8–12	No	23
$Gfap\text{-}Cre/Ptc^{C/C}$	Shh/desmoplastic	100%	3–4	No	23
$Sufu^{+/-}/P53^{-/-}$	Shh/desmoplastic	58%	by 28	No	25
Hemizygous ND2-SmoA	Shh/desmoplastic	48%	25	No	26
Homozygous ND2-SmoA	Shh/desmoplastic	94%	4–8	Yes	27
$Gfap\text{-}Cre/Rb^{lox/lox}/Tp53^{-/- \text{ or } lox/lox}$	Shh/desmoplastic	>84%	12	No	30
$Lig4^{-/-}/p53^{-/-}$	Shh/desmoplastic	100%	3–9	No	32
$Nestin\text{-}Cre/Xrcc4^{lox/lox}/p53^{-/-}$	Shh/desmoplastic	87%	12–14	No	33
$Nestin\text{-}Cre/Xrcc2^{lox/lox}/p53^{-/-}$	Shh/desmoplastic	>90%	14–16	No	34
$Nestin\text{-}Cre/Lig4^{lox/lox}/p53^{-/-}$	Shh/desmoplastic	>90%	14–16	No	34
$Nestin\text{-}Cre/Brca2^{lox/lox}/p53^{-/-}$	Shh/desmoplastic	>90%	14–16	No	34
$Parp1^{-/-}/p53^{-/-}$	Shh/desmoplastic	49%	8–24	No	36
GTML	Classic or LCA	75%	by 29	Yes	37
$Blbp\text{-}Cre/Ctnnb1^{+/lox(ex3)}/Tp53^{fix/fix}$	Wnt-subgroup	15%	~41	No	39

Table 1 Medulloblastoma genetically engineered mouse model (GEMMs).

The first mouse model that was generated to elucidate the Shh signalling role in Medulloblastoma pathogenesis is a transgenic mice haploinsufficient for Ptch1 ($Ptch^{+/-}$). In 1997, Goodrich et al. identified that the homozygous deletion of one part of the first exon (including the putative start codon) and the whole second exon of Ptch1 is embryonically lethal. The deletion in heterozygosis leads to Medulloblastoma formation with a penetrance

of 14%, starting around five weeks after birth with a peak of incidence between 12 and 25 weeks (Goodrich et al., 1997). Similar results have been obtained by generating a mouse replacing exon 6 and 7 of Patched with a neomycin resistance cassette (Hahn et al., 1998). After further characterizing the first generation of the Ptch+/- mouse model, Wetmore et al. demonstrated that genomic instability may contribute to the pathogenesis of MB, crossing Ptch+/- mice with Tp53 deficient mice (Tp53-/-), which dramatically increase MB incidence to over 95% and reduced the latency to 12 weeks after birth, (Wetmore et al., 2001).

The Cre-loxP system was employed to generate a second generation of Ptch mouse model to determine exactly which type of cell give rise to the Medulloblastoma Shh dependent. To specifically marker the PTCH loss in GCPs, Yang et al., generated a conditional Ptch1 knockout mouse crossing a $Math1^{Cre}$ transgenic mouse with a $Ptch1^{Flox}$ mice. These $Math1^{Cre}/Ptch1^{Flox}$ mice develop Medulloblastoma between week 8 and 12 with a total penetrance, strongly suggesting that GCPs are the cells from whom Shh Medulloblastoma arise. In parallel, they generated $Gfap^{Cre}/Ptch1^{Flox}$ mice, in which Ptch1 is deleted in neuronal stem cells and develop Medulloblastoma between 4 and 14 postnatal days with a latency of 3-4 weeks (Yang et al., 2008).

Different Hh models have been used to demonstrate a role of the Hh pathway in cerebellar foliation pattern (Sudarov et al., 2007). The cerebellum displays a complex three-dimensional structure with the antero-posterior axis divided in lobules with distinct sizes and the foliation pattern differs along the mediolateral axis defining a medial vermis and two lateral hemispheres.

In the vermis, lobules are further grouped into four antero-posterior zones based on specific gene expression patterns: the anterior (AZ, lobules 1-5), central (CZ, lobules 6-7), posterior (PZ, lobules 8 and anterior 9) and the nodular zones (NZ, posterior lobule 9 and 10). The

shape and sizes of lobules are different, but the overall foliation pattern is highly conserved within a species and throughout mammals, suggesting an orchestrate mechanism under genetic control (Sudarov et al., 2007).

Foliation in the mouse begins at E16.5 with the sequential formation of the base of each fissure, which have been termed "anchoring centres" (Sudarov et al., 2007). Recent studying has been demonstrated that granule cells production is differentially regulated in each of the four anterior-posterior zones of the medial vermis. In particular, the timing of granule cells production is specific to each lobule, and the lobules grow out away from anchoring centres. The first sign of an anchoring centre formation is an inward thickening of the EGL that is followed by formation of an indentation of the cerebellum outer surface and elongation of the GCPs bodies (Sudarov et al., 2007; Cheng et al., 2010).

In the mouse vermis, the homeobox engrailed genes (En1/2) are fundamental for the patterning process as they determine four initial anchoring centres, which will define five initial lobes, which are further subdivided in ten lobules (Sudarov et al., 2007; Cheng et al., 2010). Legué et al. have demonstrated that the timing of granule cells production diverges more between zones than between lobules within a zone (Legué et al., 2016). They show that granule cells production is almost complete at P14 in lobules of the AZ, PZ and NZ; whereas more than 10% of granule cells are produced after P14 in the CZ (Legué et al., 2016). In this contest some questions remain unsolved, such as which is the genetic pathways that regulate the formation of distinct lobules in the vermis and the hemispheres, and which cell type starts anchoring centres formation such as how they are positioned.

To determine when and where the Shh signalling pathway might function during cerebellar foliation pattern, mouse models Shh-deficient and a mouse model with aberrant activation of the Shh pathway have been generated (Lewis P. et al; 2004; Corrales et al., 2004).

Mice Shh^{c}/Shh^{n}-$Pax2^{Cre}$ and Shh^{c}/Shh^{n}-$L7^{Cre}$ loose Shh expression during early stage of embryogenesis and around birth respectively. In both these mutants, the EGL was thinner at E18.5 and failed to expand by P5, Purkinje cells were present but failed to form monolayer, the IGL was absent (Shh^{c}/Shh^{n}, Pax2-Cre) or sparsely populated (Shh^{c}/Shh^{n}, L7-Cre), and the caudal lobes were better organized than rostral lobes (Lewis P. et al; 2004).

On the contrary, the overexpression of Shh induces alterations in cerebellar foliation, in particular, causes expansion of the folia and IGL (Corrales et al., 2004). Interestingly, increased levels of Shh in the cerebella of Shh-P1 transgenics mice result in overall enlargement of the cerebellum but not in MB development. In addition, there is a greater thickening of the IGL and distinct bulges in the anterior vermis, where Shh levels are highest and maintained over the longest time period during development. The basic foliation pattern, however, is intact but histological analysis revealed a thicker IGL in lobes III, IV, V and IX (Corrales et al., 2004). These observations confirm the relevance of the Shh pathway in the cerebellar foliation patterning during both embryonic and postnatal stages.

AIM OF THE STUDY

KCASH2 takes part in the modulation of the Hedgehog (Hh) pathway, which plays a role in development, embryogenesis and tumorigenesis.

In particular, KCASH2 protein prevents the transcriptional activity of Gli1, interacting with the E3 ubiquitin Ligase Cullin 3, mediating the ubiquitin-dependent degradation of histone-deacetylase 1 (HDAC1), which would otherwise deacetylate Gli1 enhancing their transcriptional activity. KCASH2, as well as the other KCASH family members, displays reduced expression or is deleted in Hh-dependent and Hh-independent Medulloblastoma (MB).

The aim of my project is the generation and characterization of a new mouse model knocked-out of the KCASH2 gene, in order to obtain a better understanding of KCASH2 role in development and pathology. We plan to focus first on KCASH2 role as negative regulator of Hh signalling, analysing KCASH2^{KO} mice cerebellar development and the relevance of the KCASH2 as risk factor for MB tumorigenesis. Moreover, we will search for previously un-described roles of KCASH2 in the physiology and pathology of other organs and tissues.

MATERIALS AND METHODS:

Mouse Lines

KCASH2HT(C57BL/6N) mice were generated in the laboratory of Professor Pedro Moreira, European Molecular Biology (EMBL), Monterotondo (RM), by homologous recombination which specifically abolish the KCASH2 gene expression, inserting between the promoter and the first exon of KCASH2, the reporter gene β-gal followed by a polyadenylation signal sequence.

The targeting vector (Fig.1) designed in our laboratory and obtained from a KOMP Repository clone named KOMP-(PRPGS00164_A_G01-Kctd21-ampicillin) contains:

- Two homology arms of 5646 bp at 5 'and 5269 bp at 3' with the sequence of DNA target corresponding to the genomic region in which it maps the KCASH2 gene;
- A gene cassette containing the reporter gene Lac Z (gene encoding bacterial β-galactosidase) driven by an En2 SA-IRES sequence (En2 SA: splicing acceptor region of the En2 gene; IRES: Internal ribosome entry site) and followed by a sequence of polyadenylation (SV40-PA);
- A gene cassette containing the positive selection marker Neo (Neomycin resistance gene) driven by hBAct-p (human beta-actin promoter) and followed by a sequence of polyadenylation (SV40-PA);
- The two exonic sequences of KCASH2, separated by an artificial intron in which the start codon of the ATG translation is present;
- A gene cassette containing the DT-A negative selection marker (diphtheria toxin fragment A) guided by the PGK promoter (phosphoglycerate kinase) and followed by a polyadenylation sequence (SV40-PA);

- Amp-R resistance genes (ampicillin resistance) and BSd-R (Blasticidin S deaminase resistance);
- FRT sequences flanking the sequence containing the gene cassettes for the LacZ reporter gene and the positive selection marker; a Lox P sequence upstream of the gene cassette containing the positive selection marker and two Lox P sequences flanking the first exon of KCASH2; all the sequences have an orientation in the same direction to allow the deletion of the included regions.

Successfully the vector was linearized with the AsiSI restriction enzyme and was electroporated in murine embryonic stem cells (mESC C57BL/6N). Once integrated into the target site by homologous recombination in mESC was cells positively selected by culturing ESCs in medium with specific antibiotics. The identified and expanded homologous recombinant ESC clones (derived from mice with an agouti coat) are injected into recipient pre-implantation mouse embryos (blastocysts) that are collected from female mice with black coat (strain C57BL/6). These injected blastocysts are then surgically transferred to a recipient pseudo pregnant foster mother to allow the embryos to develop. Chimeric offspring are mated with C57BL/6 mice, transmitted the modification through the germ line and produce the F1 generation, mice heterozygous for the presence of the construct.

The construct was microinjected into fertilised eggs from C57BL/6JRj mice. The F1 transgenic mice were backcrossed whit the C57BL/6JRj for 10 generations to obtain transgenic mice on the C57BL/6JRj background. Production and maintenance of the transgenic line was undertaken in our animal facility by crossing heterozygous KCASH2 mice. Genotype was determined by PCR analysis of tail DNA; using PCR primers:

- 3LR KCASH2 FW: 5'-ACCAAGCAGAACCTGAAAAG-3'
- 4LR KCASH2 RV: 5'-GGGGAAACAAACACTCTCTG-3'

Animals were maintained with food and water ad libitum in a 12-h light/dark cycle during the experiment. All animal studies were conducted using the National Institutes of Health guidelines for the ethical treatment of animals with approval of the Rutgers Animal Care and Facilities Committee.

RNA preparation and Q-PCR analysis

Total RNA extraction was isolated using TRIzol reagent (Invitrogen) and analysed by quantitative real-time PCR (Q-PCR) using a 1x TaqMan Universal PCR Master Mix (Applied Biosystem). Primer for KCASH2 were:

- forward: 5'-GAGCGAGGGCAGGAGTATTTC -3'
- reverse: 5'-CCCCCAACATTCAGTGTAATGG -3'
- probe: 5'-CACCCAGCCTCCTAC-3'

Protein preparation and Western Blot

Tissue were washed with ice-cooled Phosphate-buffered saline (PBS) and homogenized in RIPA buffer (50 mM Tris-HCl pH 7.6; 1% Sodium deoxycholate, 150 mM NaCl; 1% NP40, 5mM EDTA, 100 mM NaF) with a protease inhibitor mix (40mg/ml aprotinin, pepstatin, leupeptin, 0,5 mM PMSF, Na3VO4). Proteins were quantified using the Bradford assay and equal amounts of protein were loaded on SDS gels and transferred to nitrocellulose membrane (Schleicher & Schuell, Dassel, Germany). To ensure equal protein levels, blots were stained with Ponceau before the incubation with antibodies. The blots were then rinsed and blocked in 5% no fat dried skin milk in TBS-T for 30 minutes at room temperature (RT). Blots were incubated with primary antibodies; then, washed with TBS-T 3 times for 5 minute each and incubated with secondary antibody for 45 minutes at RT. Membranes were washed 3 times for 5 minute each in TBS-T. To confirm equal protein levels, blots were reprobed

with actin. All analyses were performed at least three times in independent experiments. Antibody used were: Anti-KCTD21 (Abcam) 1:1000 O/N; Anti-Actin (Thermo Fischer) 1:10000 1h at RT; Anti-HDAC1 (Abcam) 1:1000 O/N.

β-galactosidase Staining

Brains and Cerebella in toto were removed under sterile condition from P7 (or later stages) WT and KCASH2^{KO} mice after euthanizing with CO2. The tissues were then immersion fixed in 4% Paraformaldehyde solution in PBS at RT for 16 hours. Fixed tissues were cryoprotected in 20% sucrose overnight at 4°C and embedded in OCT (Tissue-Tek).

β-gal activity was detected in 10 μm frozen sections by incubation in X-gal solution (KIT MIRUS) overnight at 37°C. β-Galactosidase catalyses the conversion from X-gal to 5-bromo-4-chloro-indoxyl, which is visible after oxidation as a blue precipitate in the cells where the reporter gene is expressed. Sections were counterstained in Nuclear Fast Red.

For the testis and epididymis cryosections we have optimise the protocol to abolish β-gal endogenous activity. The frozen sections were rinsed in the detergent rinsing buffer (0.02% Igepal, 0.01% sodium deoxycholate and 2 mM of MgCl2 in 0.1 M phosphate buffer [pH 7.5]) and immersed in staining buffer (0.02% Igepal, 0.01% of sodium deoxycholate, 5 mM of potassium ferrocyanide, 5 mM of potassium ferrocyanide and 2 mM of mgCl2 diluted in 0.1 M phosphate buffer [pH 7.5]) in which has been added 1mg/ml X-Gal dissolved in N,N-dimethylformamide directly prior to use.

Cerebellar granule cell precursors culture

Cerebella from P7 mice were minced into small pieces and rinsed in Neurobasal medium (GIBCO) containing 10μg/ml DNase (Sigma) at RT for 15 min. Single cell suspension was obtained via trituration with glass pipettes and then centrifuged at 1000 rpm for 5 min. Cells

were suspended in the GCP culture medium, which is composed of Neurobasal medium with L-glutamine, B27 supplement, penicillin/streptomycin and 5% Foetal Bovine Serum (FBS). GCPs were plated on poly-D-lysine coated dishes and were maintained in 5% CO2 at 37°C; and analysed 24h after incubation.

Histology and Immunohistochemistry analysis

Brains and Cerebella were dissected in toto and immersion fixed in 4% paraformaldehyde solution in PBS overnight at 4°C. Tissues were then embedded in paraffin according to standard methods and sectioned at 4 μm.

To recognizing morphologic changes in cerebella tissues from wild-type (WT) and KCASH2^{KO} mice, was used the Haematoxylin/Eosin standard staining.

Antibody staining was performed according to manufactory protocols and following the Mouse to mouse HRP (DAB) staining system Kit (Scy Tek Laboratories Inc.).

The following primary antibodies were used: Gli1-H300 (1:200; Santa Cruz).

Immunohistochemistry fluorescent staining

Early postnatal stages cerebella were dissected, and immersion fixed in 4% paraformaldehyde overnight at 4°C, then cryopreserved with 20% sucrose. Section (10 μm) were cut using a Leica cryostat, and mounted onto charged slides.

For Immunofluorescences the sections were permeabilized with 0,2% triton in PBS for 10 minutes and blocked with 3% BSA and 5% goat serum in PBS (Block Solution) for 1 hour at room temperature. Primary and secondary antibodies were prepared in block solution. Sections were incubated with primary antibodies overnight at 4°C in a humidified chamber.

Antibody used were: Ki67 (1:500, Santa Cruz), HDAC1 (1:300, Abcam), Calbindin (1:500, Sigma).

All secondary antibodies were diluted (1:1000) and incubated for 1 hour at RT. Nuclei were labelled with Hoechst in PBS for 5 min at RT. Controls for the immunostaining were incubated with secondary antibodies without primary antibodies.

Thickness quantification of the inner granule layer (IGL)

To quantify IGL thickness, high magnification images were taken of medial section from wild-type (WT) and mutant cerebella KCASH2^{KO}. The area encompassed by the IGL in sagittal section was calculated using ImageJ software. Three different sections from the same samples (the most medial 10 μm) were used to measure mutant and control.

Behavioural analysis

During Morris water maze Test (MWM), the mice were placed in a circular white pool (diameter 140 cm) filled with 24°C water made opaque by the addition of atoxic acrylic colour (Giotto, Italy), at different starting point for each trial, and have to use the spatial layout of the room to navigate to the platform that is kept in a constant location. These learning trials is called Cue phases. During the Cue Phase an escape platform (diameter 10 cm) was placed in the centre of the pool and emerged 2 cm above the water level. Each mouse was submitted to an 8-trial Cue phase with an inter-trial interval of 15 min. The mouse was released into the water from randomly varied starting points and allowed to reach the platform for a maximum of 60 s. When the mouse reached the platform, it was allowed to remain there for 30 s. If the mouse failed to reach the visible platform within 60 s, it was gently guided there by the experimenter.

In the following three days, each mouse was submitted to a 15-trial Place Phase (5 trials/day), in which the procedures were the same used during the Cue phase, but the escape platform

was submerged 2 cm below the water level and placed in the middle of NE quadrant of the pool. The day after the end of the Place Phase, the mice were submitted to 1-trial Probe Phase, in which the platform was removed, and the mice were allowed to swim for 30 s in searching for it.

Throughout the entire test, navigational trajectories were recorded by a video camera whose signal was relayed to a monitor and to the image analyser (Ethovision, Noldus, Wageningen, The Netherlands).

As for females and males separately, the following MWM parameters were considered as indices of learning during Cue and Place Phase: latencies (in sec) to find the platform; total distance (in cm) swum in the pool; mean swimming velocity (in cm/sec); the percentage of navigational strategies put into action in reaching the platform. The navigational strategies were classified in three main categories, regardless the platform was reached or not: Extended Searching, swimming around the pool initially with circular trajectories and then exploring the whole pool area; Restricted Searching, swimming in only some pool quadrants, not visiting other areas; Finding, swimming toward the platform without any foraging around the pool. Two researchers unaware of the individual specimen's phenotype categorized the swimming trajectories drawn by the image analyser. They attributed the dominant behaviour in each trial to a specific category (inter-rate reliability > 0.85). Furthermore, the percentage of the total distance swum in the previously rewarded (platform) quadrant during Probe Phase was considered as a spatial memory index.

The Rotarod Test was performed by using a device consisting of a computerized electronically controlled system (Panlab, Harvard Apparatus), composed of a four-lane suspended rotating drum (3 cm in diameter), whose surface was manufactured to provide grip for the animal. The apparatus was set up in an environment with minimal disturbances. Each animal is placed on the rotating lane, when the animal drops into its own lane, the time

latency to fall (seconds) and rotation speed (rpm) are automatically recorded. A removable upper separator is included to prevent interference between animals running in adjacent lanes. Mice were acclimated to the stationary rod for 30 seconds on the first day of the test. Then, rotation was electronically settled at a linear acceleration rate (4-40 rpm) in 300 seconds. Each trial lasted for a maximum of 300 seconds and mice were rested for minimum 5 min between trials to avoid fatigue. Mice underwent three trials per day for four consecutive days.

Statistical Analyses

Statistical analyses on behavioural analysis were performed by using STATISTICA 8.0 (StatSoft, Italy). The data expressed as mean ± SEM were firstly tested for normality (Wilk–Shapiro's test) and homoscedasticity (Levene's test). Given that parametric assumptions were not fully met, non-parametric analyses of variance (Friedman's test, Wilcoxon's test and Mann–Whitney's U test) were used. Square root transformations were computed on the percentage of navigational strategies and distance swum during Probe Phase. Differences were considered significant at the $p < 0.05$ level.

For all the other assays, experimental groups were compared using student's t-test, as appropriate, $p<0,05$ was considered significant.

RESULTS:

Generation of the KCASH2^{KO} mouse

To understand the role of KCASH2 as a negative regulator of the Hedgehog pathway *in vivo* during development, differentiation and tumorigenesis, we have generated the new KCASH2^{KO} mouse model. To this end, we have used a targeting construct containing the LacZ reporter gene cassette, followed by a polyadenylation signal sequence, flanked by 5' and 3' homology arms as illustrated in Fig.8.

The correct insertion of the cassette in the target genomic sequence generates a knocked-out phenotype, since the endogenous promoter drives the transcription of the lacZ reporter gene cassette, but the presence of a stop and the polyA sequence does not allow the transcription and translation of the KCASH2 mRNA. The linearized targeting construct was electroporated into Embryonic Stem Cells (ESCs) from C57BL/6 mice, and recombinant ES cells were screened, and positive ES injected into host embryos, to generate chimeric mice and finally positive heterozygotic pups.

KCASH2^{KO} mice were obtained by crossing the heterozygous mice, and genotype was confirmed by PCR on genomic DNA extracted by small tail biopsies (Fig.8 panel B; Primers used for genotyping are shown in Fig.8 panel A).

After genotypization, we also confirmed the loss of KCASH2 gene expression in adult cerebella by evaluating mRNA expression (Fig.8 panel C) and protein levels (Fig.8 panel D). As expected, KCASH2^{KO} mice do not present any RNA and protein expression.

KCASH2^{KO} mice were born at the expected Mendelian ratio from heterozygous parents. They did not present gross abnormalities and were able to breed.

We are currently maintaining KCASH2^{KO} and WT sibling controls in order to evaluate the incidence of Medulloblastoma. The first group of four KO mice has reached the age of 1

year without evidences of MB formation. Of course, data are not yet conclusive, and we are increasing the cohort of animals analysed to obtain a statistically relevant sample size.

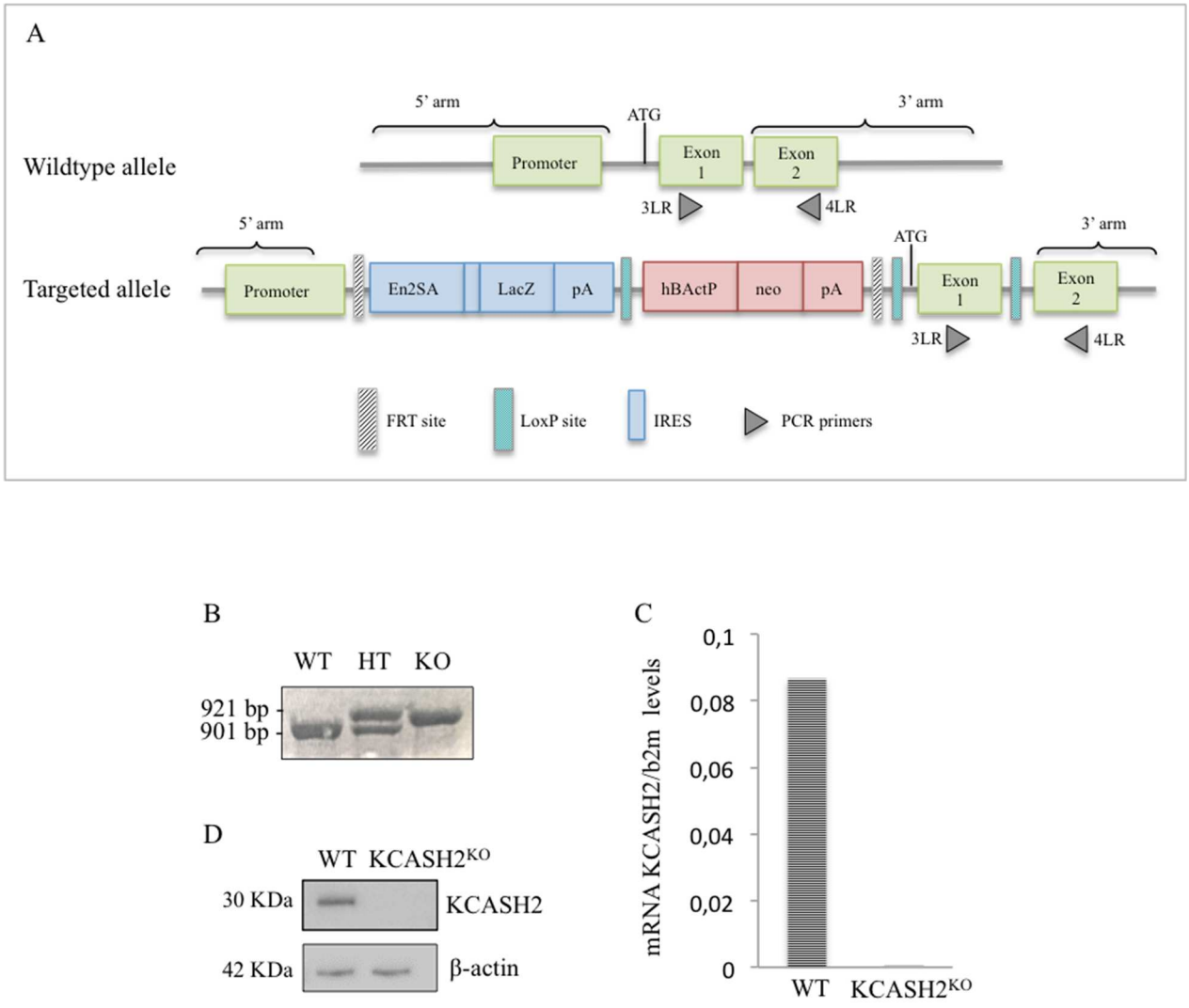

Fig.8 Generation of mutant KCASH2^{KO} mice from genetically modified embryonic stem cells. (A) Schematic representation of the vector used to generate the "Knock-out first" mouse by homologous recombination. (B) Mouse genotyping by PCR analysis, using the indicated PCR primers in (A). Lanes: wild-type (WT), heterozygous (HT) and homozygous (KO). (C) KCASH2 transcript levels in the cerebellum of Adult KCASH2^{KO} and WT mice. (D) Western Blot for KCASH2 confirm absence of protein in the KCASH2^{KO} adult cerebellum.

KCASH2 expression during mouse cerebellar development

The most relevant biological function attributed to KCASH2 is downregulation of the Hh pathway in the context of cerebellum and MB.

For this reason, we have first assessed the LacZ-reporter expression, which is driven by the KCASH2 promoter, in adult KCASH2^{KO} mice cerebella cryosections (**Fig.9**, panel A), confirming expression in cerebellum, and in particular in differentiated cerebellar granule neurons in the IGL.

We decided to evaluate the physiological levels of KCASH2 expression during postnatal development in mouse cerebellum, analysing mRNA and protein levels in wild type mice cerebella. Evaluation of KCASH2 mRNA levels, was performed in total mRNA extracts at different postnatal ages (P7, P14, P21 and P28), confirming modulations in mRNA levels during cerebellar development, and revealing the highest levels of expression around P21, when almost all the granule cell precursors have migrated to the IGL and have differentiated in mature granule cells (**Fig.9**, panel B).

This result indicates that during early postnatal development the expression of KCASH2 mRNA is at the minimum, while in the late development phases, when the Shh pathway switch off, the differentiation process begins, the KCASH2 expression increases reaching a basal level that is maintained until the adulthood (**Fig.9**, panel B).

KCASH2 protein levels, evaluated by western blot of cerebellum lysates from different postnatal ages confirmed the modulation of KCASH2 during development; and indicated that its expression is minimal at P7 but increases from P14 and reaches a maximum starting from P21 to adulthood (**Fig.9,** panel C), coherently with KCASH2 role as suppressor of Hh signaling pathway.

Similar results were obtained by analysis performed on cryosections from KCASH2^{KO} P7, P21 and Adult mice cerebella, which were stained with the X-gal assay (Fig.9, panel D).

As expected, LacZ-reporter gene expression, driven by KCASH2 promoter, is present in the cells of the cerebellar internal granular layer (IGL) confirming the specific expression in the expected cell type, which respond to the Shh signaling (Lewis et al., 2004) and, surprisingly, in Purkinje cells (PL) (Fig.9, panel D).

To confirm specificity of KCASH2 expression in granule cells we performed cerebellar granule precursors primary culture and analysed KCASH2 protein levels by western blot. As shown in Fig.10, panel A, KCASH2 protein is detected in the granule primary culture obtained from P7 WT cerebella at, while is absent in primary cultures from KCASH2^{KO} mice (Fig.10, panel A).

To confirm KCASH2 role in modulating the Hh pathway to determinate granule cells maturation and differentiation, we compared expression of Gli1 (the primary target and transcription factor of the Shh signaling) in cultured granules derived from WT and KCASH2^{KO} mice (Fig.10, panel B). The quantitative analysis showed a clear difference in Gli1 levels, indicating that the absence of KCASH2 resulted in an over-activation of Gli1 transcription factor and the consequent Shh over-expression in KCASH2^{KO} granule cells.

To better understand the significance of KCASH2 expression in Purkinje cells we decided to evaluate the levels of HDAC1 protein in these cells. In fact, while there are not previous evidences of Gli expression in Purkinje cells, there are hints that HDAC1 may be modulated in Purkinje during cerebella maturation. Double immunohistochemical labelling experiments with anti-HDAC1 and anti-Calbindin (Purkinje cells marker) antibodies show that in the adult KCASH2^{KO} Purkinje cells express higher levels of HDAC1 compared with WT (Fig.11).

This data is coherent with our data, as (De Smaele et al. 2011), showing that HDAC1 protein levels are maintained low through the activation of KCASH2, which acts as an adapter between HDAC1 and Cul3-E3 ligase to induce HDAC1 ubiquitination and its proteasomal degradation.

It remains to be investigated the physiological effect of this altered HDAC1 protein level in Purkinje cells.

Therefore, our experimental results seems to be coherent with data from literature which show that the post mitotic migrating neuronal cells of the cerebellar cortex, mature granule cells and Purkinje cells show weak Gli1 and HDAC1 levels expression (De Smaele et al., 2008; Yoo JY., Larouche M. and Goldowitz D., 2013), while the our mouse model show a high Gli1 and HDAC1 level, enhancing Hedgehog pathway activity

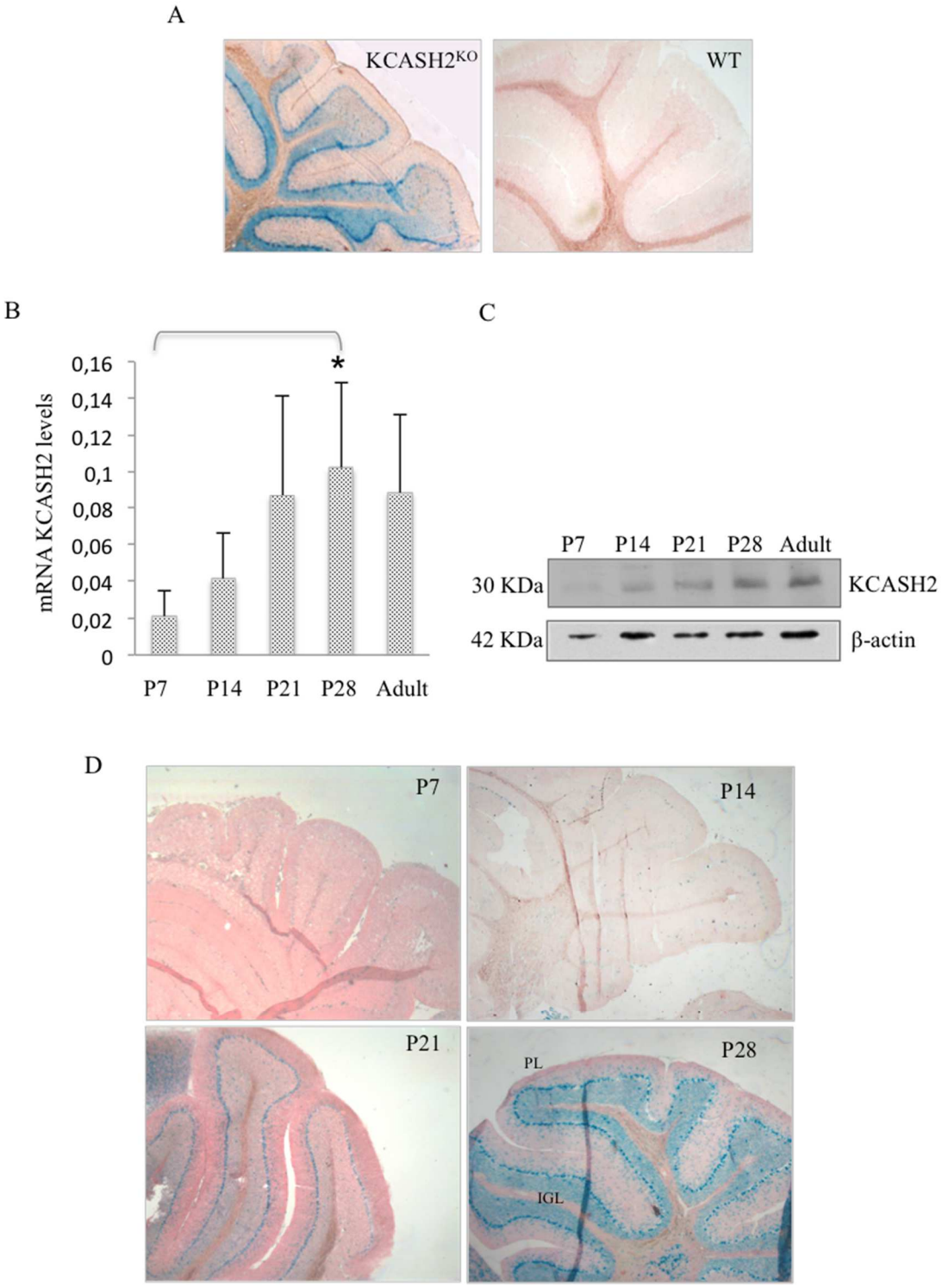

Fig.9 KCASH2 expression levels is modulated during development and differentiation of mouse cerebellum. (A) βGal reporter gene expression in the adult KCASH2^{KO} mice cerebellum compared to the negative controls adult WT. (B) KCASH2 expression levels in total cerebellum lysate from mice at different ages from P7 to Adult. (C)Western Blot of KCASH2 in cerebellar lysates from the indicate postnatal ages. (D) Expression pattern of βGal activity from the KCASH2 locus during cerebellum development. The panel reveals positive KCASH2 signaling in area corresponding to PL and IGL. PL = Purkinje cells layer; IGL = internal granule layer.

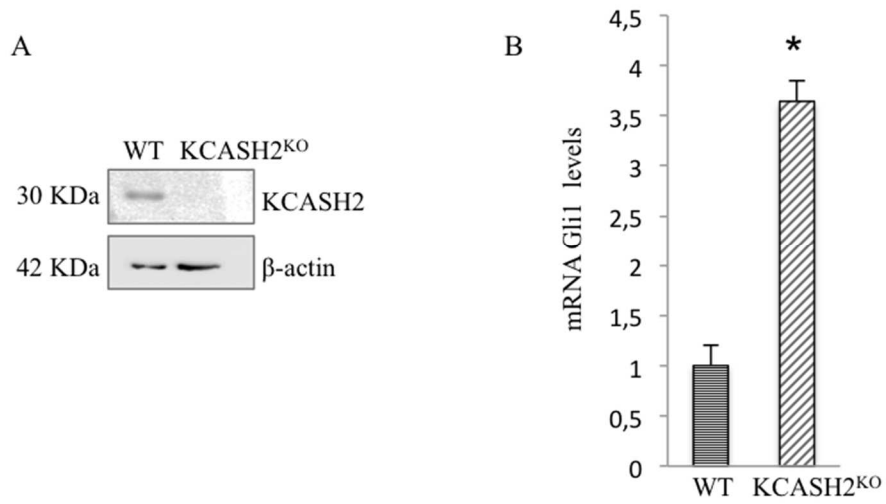

Fig.10 KCASH2 expression in granule primary culture.
(A) Western Blot of granule primary cultured from P7 mice cerebellum. (B) Difference in Gli1 transcript levels between granule primary cultured WT and KCASH2^{KO} are evident. * P<0.05.

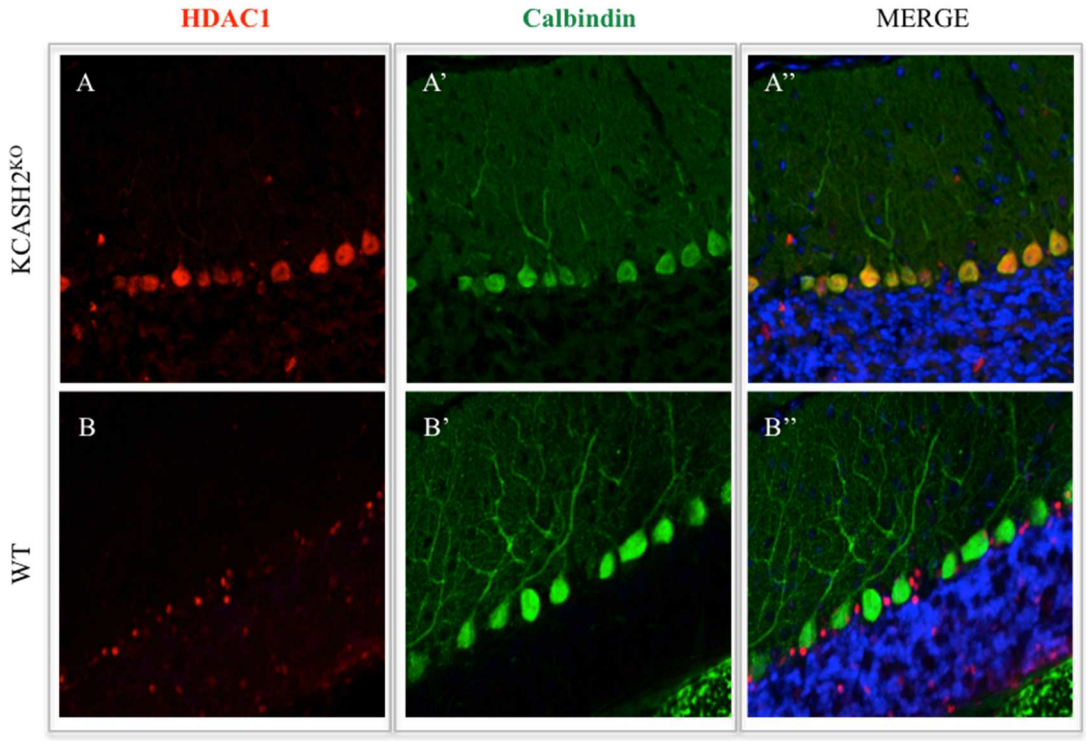

Fig.11 HDAC1 expression in KCASH2^{KO} mice.
HDAC1 labelling (A-B) in adult sagittal cerebellar sections shows high HDAC1 expression in Calbindin-expressing Purkinje cells in KCASH2^{KO} mice (A'-A''), in contrast with control which express low HDAC1 levels (B'-B'').

KCASH2 loss induces a thicker Inner Granule Layer in the IV-V folia,

After verifying that in the KCASH2^{KO} mouse the Shh pathway is more active, to determine if KCASH2 loss can affect in vivo cerebellar development, we compared several KCASH2^{KO} and WT adult mice cerebella.

Evaluation of gross morphology of cerebella from adult WT and transgenic mice does not highlight differences. Histological analysis shows that the basic foliation pattern in KCASH2^{KO} mice appears intact but reveals also a generally thicker IGL compared with WT (Fig.12). The IGL is thickest in IV-V lobes (statistically significant), which correlates with the normal expression pattern of Shh. Measurements of the area occupied by the IGL in KCASH2^{KO} mice, show a 10% overall increase compared with those of WT (Fig.12).

Interestingly, this phenotype strongly resembles the previously described phenotype exhibited by Shh-P1 mice, which present an increased expression of Shh protein and Gli1 activity (Corrales et al., 2004;).

Our result can be explained based on previous data from literature. Indeed, it has been demonstrated, that in the anterior vermis (lobes I-V) Shh levels are highest and maintained over the longest time period during development respect to the central/posterior vermis (Corrales et al., 2004).

Therefore, that the loss of the negative regulation in the KCASH2^{KO} mice maintains the Shh signaling active in these regions and leads to a prolonged proliferation of neuronal granule cell precursors (GCP) during the earlier times of cerebellar development.

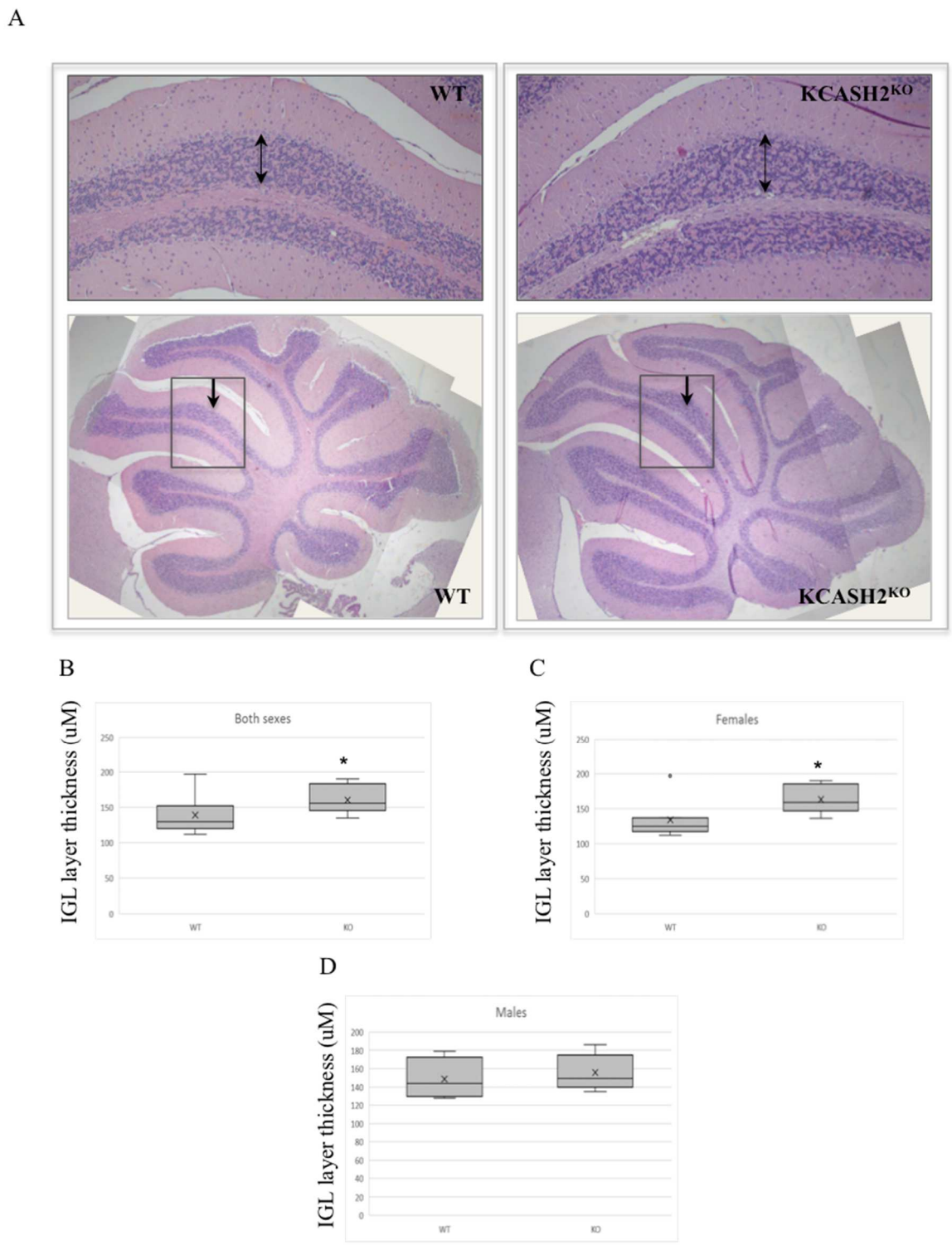

Fig.12 KCASH2 loss affects cerebellar morphology, inducing a thicker Inner Granule Layer in the IV-V folia. (A) Midsagittal section of WT and mutant cerebellum adult appears morphologically similar; but the mutant IGL (of IV-V lobules) is significantly thicker compared with WT (arrow). (B, C and D) Measurement of thicker IGL WT and KCASH2^{KO}. The analysis was conducted on 11 animals for each group (WT and KCASH2^{KO}). * significantly different from WT at $p < 0.05$.

KCASH2 is involved in regulation of GCPs proliferation

Shh is a well-established mitogen for GCPs, and previous studies have shown that P5-6 is the time of maximal GCP proliferation. After P7, two sublayers became apparent in the EGL: the external zone, where GCPs continued to proliferate, and internal zone where the cells start to differentiate and migrate to the IGL. In the WT mice the number of proliferating GCPs in the EGL began to decrease at P10 and continued to decrease until few proliferating cells remained in the EGL at P14.

We hypothesize that, in our mouse model KCASH2^{KO}, the thickening of the IV-V is a consequence of the delay in the depletion of the EGL and therefore of a prolonged proliferative phase of the GCPs. To verify this hypothesis, we decided to monitor the number of proliferating cells during postnatal cerebellar development (Fig.13).

By labelling cerebellar cryosections whit antibody Ki67, a proliferation marker, we observed that in KCASH2^{KO} mice at P7 and P10, the number of Ki67+ cells in the EGL was higher than WT; while at P14 the Ki67 positive cell number was similar in WT and KO (Fig.13).

This indicates that proliferating GCPs decrease in EGL of WT mice more quickly than in in KCASH2^{KO} mice, that retains a higher proliferation rate.

To confirm that the absence of KCASH2 resulted in highest Shh pathway activation in this timeframe, we performed antibody staining with Gli1 and discovered that GCPs in the KCASH2^{KO} mice at P10 maintain Gli1 high levels in correspondence of EGL plica IV-V, showing three to four layers of cells in the KCASH2^{KO} mice compared with a single cell layer in the WT mice (**Fig.14**, panel A). Furthermore, we evaluate also the Gli1 mRNA in cerebellum P7, P10 and P14. As show in Fig.14, panel B, the Gli1 transcript is more active in KCASH2^{KO} mice in the early stage of development.

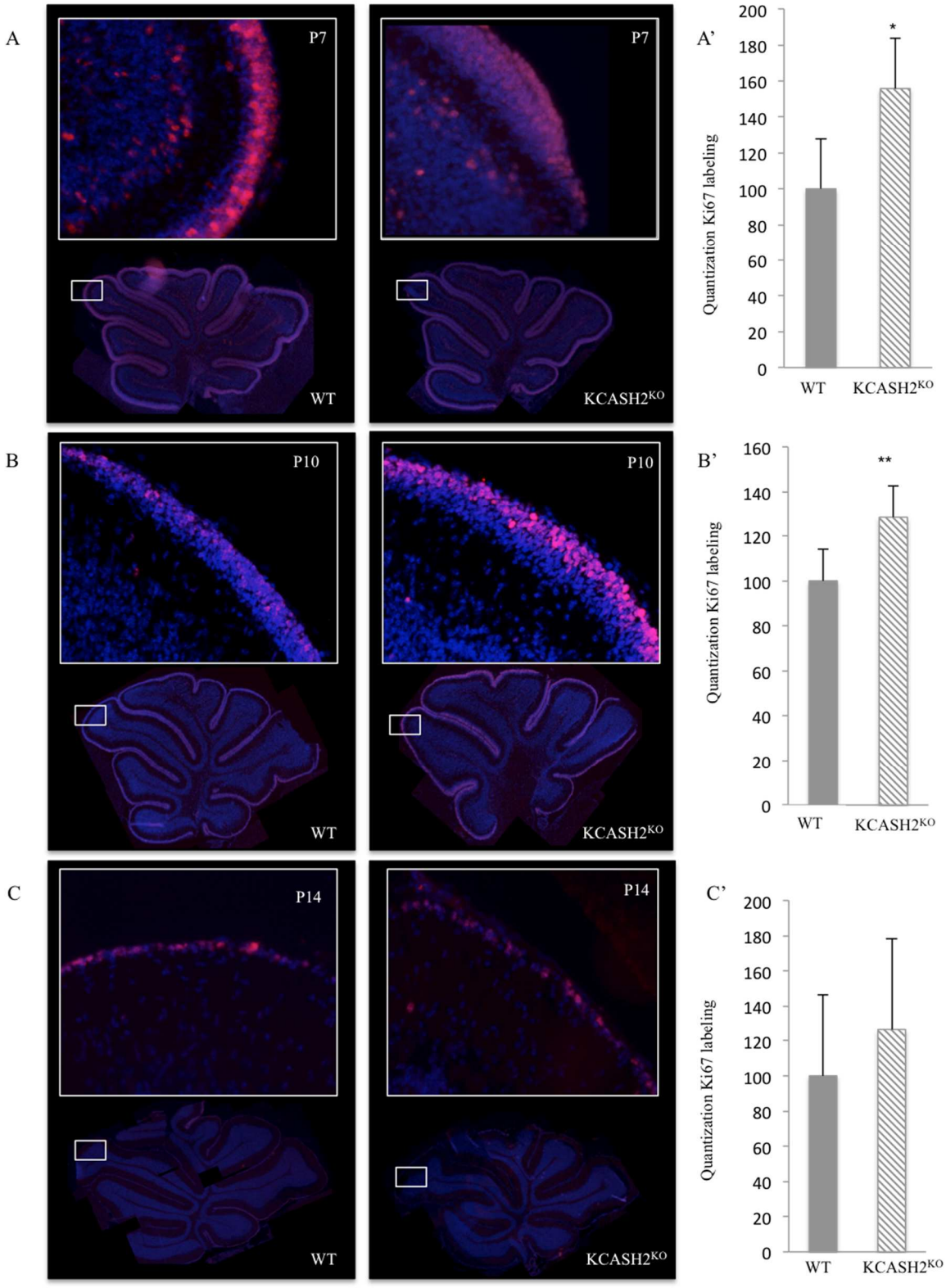

Fig.13 KCASH2 loss increases GCP proliferation. (A-C) Proliferation (assessed by Ki67 labelling) in the EGL is increased in KCASH2^{KO} mice. (A' and B') Quantification of fluorescence intensity of Ki67 staining in IV-V lobe of the EGL at P7 and P10 illustrated the markedly increased proliferation in the EGL of mutant mice. (C') There is no statistically significant difference between KCASH2^{KO} mice and WT at P14. Data are presented as mean and standard deviation; Student's T-Test was used for statistical analysis. * $P< 0.05$ and ** $P < 0.01$ was considered statistically significant.

Our observations indicate that KCASH2 deficiency increased granule cells precursor proliferation although this phenomenon restricted to a specific temporal range and limited to the anterior part of the vermis (I-V lobules). This can be explained with literature data that have demonstrated the timing of maximum production of GCPs in individual lobules, in particular, in lobe IV-V the major GCPs accumulation happens at early stage between P6 and P8, the proliferation began to decrease at P10, and continued to decrease until P14 (Legué et al., 2016). The delayed GCP production in the KCASH2^{KO} mutant mice correlates with an increment of the number of GCPs Ki67^{+} cells at early postnatal age, with persistent Shh activity and with thicker IGL in the adult.

These observations enable us to suppose that the loss of the KCASH2 gene can determine alterations in the cells proliferation in which it is expressed, but this difference between mutant and WT mice become less severe at P14. We hypothesized that KCASH2 loss can be compensated during the latest stages of development by the increased expression of the other KCASH family members, which are able to bind Cul3 Ubiquitin Ligase and induce HDAC1 proteasome degradation. Firstly, we analysed KCASH1 levels during development of WT and KCASH2^{KO} mice (Fig.15, panel A). Quantitative analysis showed a clear difference in KCASH1 levels in WT compared to KO mice, indicating that, in vivo, the absence of KCASH2 resulted in over-expression of KCASH1 transcription factor (Fig.15, panel A). Secondly, we have also evaluated the KCASH3 levels (Fig.15, panel B). As expected, the KCASH3 levels are comparable between WT and KCASH2^{KO} mice; due to the fact that KCASH3 is unable to bind directly HDAC1 protein but is able to do it only following the heterodimerization with KCASH1 (Fig.15, panel B).

Furthermore, we analyse the HDAC1 levels during WT and KCASH2^{KO} mice development (Fig.16). Western blot analysis shows a clear difference of the HDAC1 levels at P14 and P21 in WT mice compared to the KCASH2^{KO}; indicating the Shh pathway is still activate

in mutant mice until P21 (Fig.16). At P28, this difference becomes less strong due to the enhanced activation of KCASH1 which re-establishes the SHH physiological inhibition.

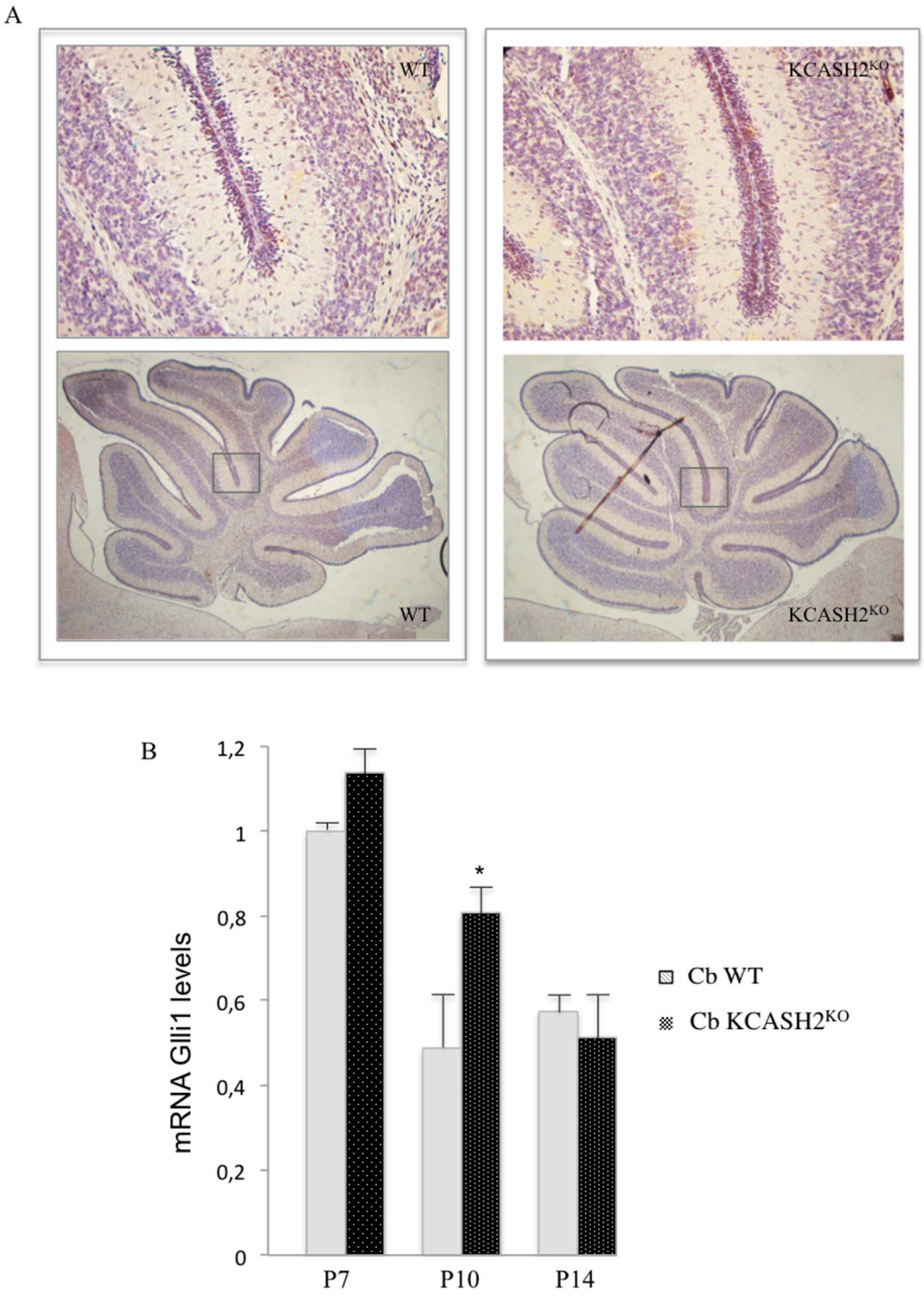

Fig.14 GLI1 levels in KCASH2^{KO} mice. (A) Antibody staining for Gli1 at P10 show the presence of major proliferating cells in EGL of mutant mice respect to WT. (B) Relative Gli1 mRNA levels in cerebellum WT and KCASH2^{KO} at different postnatal ages. * P< 0.05.

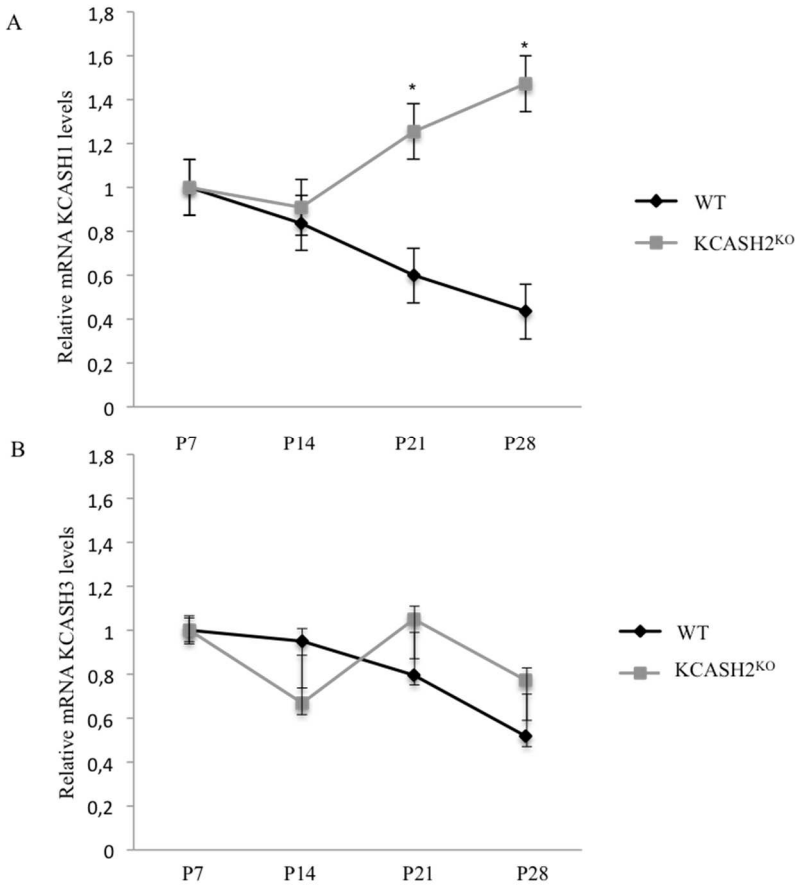

Fig.15 KCASH2 loss increases KCASH1 expression.
(A) Relative KCASH1 mRNA levels in CB development WT and KCASH2^{KO} at the indicated postnatal age. (B) Relative KCASH3 mRNA levels during CB development WT and KCASH2^{KO} at the indicated postnatal age. * P< 0.05.

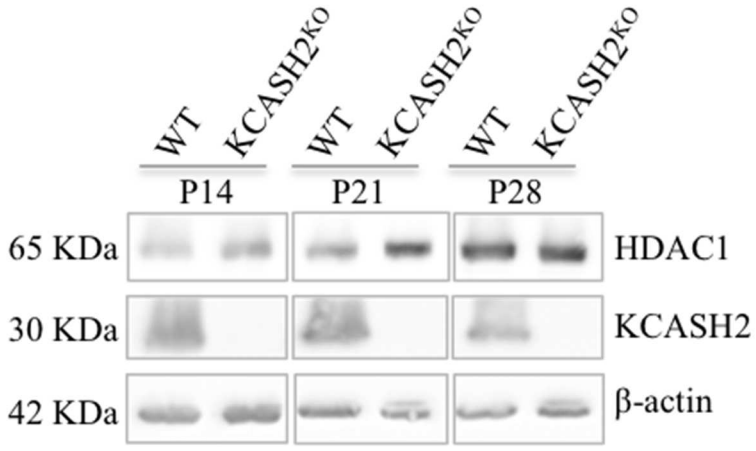

Fig.16 HDAC1 levels in WT and KCASH2^{KO} mice cerebellum.
Western Blot showing the comparison of HDAC1 expression in WT or KCASH2^{KO} cerebella at the indicated postnatal age.

KCASH2 expression in brain tissues

The reporter gene expression in KCASH2^{KO} mice reveals cellular localization in adult cerebral cortex and in hippocampus, suggesting that KCASH2 may play an important role in the CNS (**Fig.17**, panel A, B). WB confirmed the expression of KCASH2 in adult brain tissues from mouse whole brain lysates at different ages (**Fig.17**, panel C).

The expression of KCASH2 in the hippocampus and cerebellum have risen the question if KCASH2 may be involved in CNS function such us spatial memory and spatial learning and motor balance (Lackey et al., 2018).

To verify this hypothesis, in collaboration whit the laboratory of Prof. Laura Petrosini, we have performed several behavioural tests. In particular the Morris water maze (MWM) and the Rotarod tests, which are designed to verify the presence of specific functional deficits in few well-defined brain regions.

The MWM performance appears to depend upon the coordinated action of different CNS regions constituting a functionally integrated neural network; for example, the integrity of the hippocampus is essential for spatial memory; while the cerebellum is involved in spatial learning (Kipnis, Gadani and Derecki, 2012).

The Rotarod Test is a test of motor coordination, useful to test for strength and balance, which relays mainly on integrity of cerebellar functions (Heshmati and Russo, 2013).

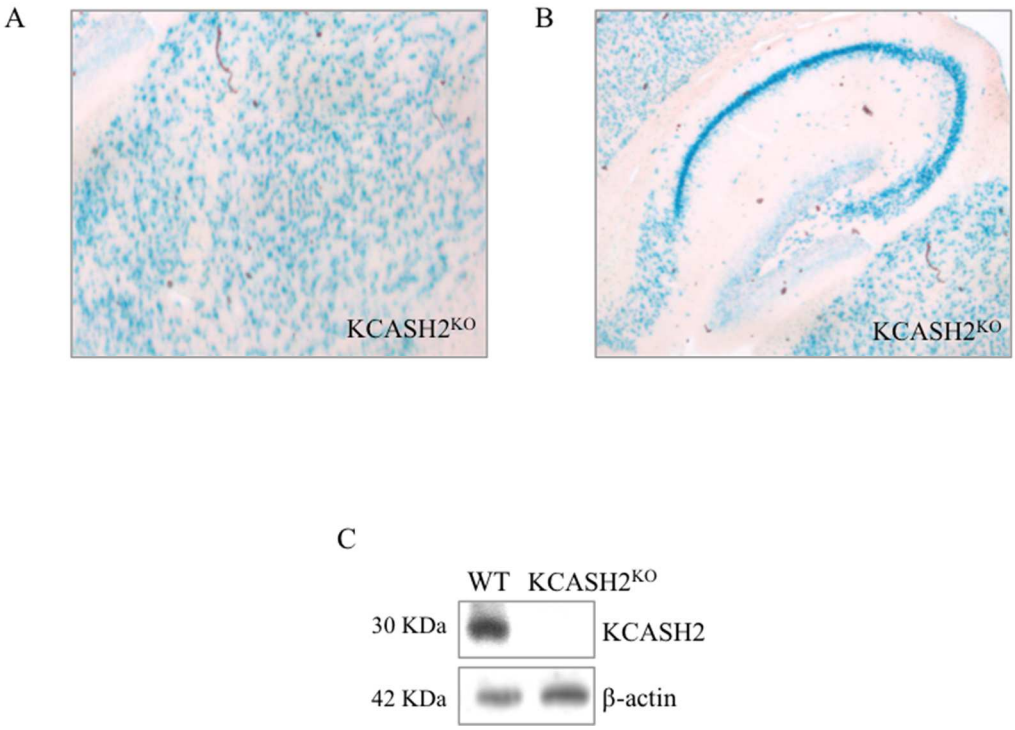

Fig.17 KCASH2 expression in the brain.
Expression pattern of βGal activity; the panel reveals positive KCASH2 signaling in cerebral cortex (A) and hippocampus (B) of $KCASH2^{KO}$ mice. (C) Western Blot of KCASH2 in the brain of Adult $KCASH2^{KO}$ and WT mice.

Behavioural observations on the KCASH2^{KO} mice suggest an abnormal cerebellar phenotype in female mice

We subjected KCASH2^{KO} and KCASH2^{WT} mice to the MWM test apt to evaluate mnesic (localizatory competencies) and procedural (navigational strategies) performances and identify animals with cerebellar or hyppocampal alterations (Federico et al., 2006; Foti et al., 2011; Gandhi et al., 2000; Laricchiuta et al., 2016; Leggio et al., 1999; Petrosini et al., 1996).

The Morris water maze (MWM) is a test of spatial learning for rodents that relies on distal cues to navigate from start locations around the perimeter of an open swimming arena to locate a submerged escape platform (Vorhees and Williams, 2006).

Spatial learning is assessed across repeated trials and reference memory is determined by preference for the platform area when the platform is absent. Reversal and shift trials enhance the detection of spatial impairments. Trial-dependent, latent and discrimination learning can be assessed using modifications of the basic protocol. Search-to-platform area determines the degree of reliance on spatial versus non-spatial strategies. Cued trials determine whether performance factors that are unrelated to place learning are present.

The following MWM parameters were considered (for females and males separately) as indices of learning during both Cue and Place Phases: latencies (in sec) to find the platform; total distance (in cm) swum in the pool; mean swimming velocity (in cm/sec); the percentage of navigational strategies put into action in reaching the platform.

The navigational strategies were classified in three main categories, regardless the platform was reached or not: Extended Searching, swimming around the pool initially with circular trajectories and then exploring the whole pool area; Restricted Searching, swimming in

only some pool quadrants, not visiting other areas; Finding, swimming toward the platform without any foraging around the pool.

Two researchers, unaware of the individual mouse phenotype, have categorized the swimming trajectories drawn by the image analyser. They attributed the dominant behaviour in each trial to a specific category (inter-rate reliability > 0.85).

Furthermore, the percentage of the total distance swum in the previously rewarded (platform) quadrant during Probe Phase was considered as a spatial memory index.

Performances in the Cue Phase

Females

Non-parametric analyses (Friedman's test) on Latencies revealed that both WT and KO groups significantly reduced the times to reach the platform as trials went by (KF-WT: Chi Sqr=16.71; p=0.001; KF-KO: Chi Sqr=12.46; p=0.006) (**Fig.18**, panel A), indicating learning capabilities. Mann–Whitney's U test did not reveal significant differences between WT and KO (trials 1-2: U=16.00; p=0.46; trials 3-4: U=15.00; p=0.39; trials 5-6: U=15.00; p=0.39; trials 7-8: U=20.50; p=0.94).

Friedman's test on Total Distance travelled revealed that both groups significantly reduced the path to reach the platform as trials went by (WT group: Chi Sqr=15.86; p=0.001; KO group: Chi Sqr=8.60; p=0.03) (**Fig.18**, panel C). Again, Mann–Whitney's U test did not reveal significant differences between WT and KO in trials 1-2 (U=19.00; p=0.77), 3-4 (U=13.00; p=0.25) and 5-6 (U=13.00; p=0.25), while the difference became close to significant in trials 7-8 (U=8.00; p=0.06).

Only in KO group there was a significant difference among the Navigational Strategies used to perform the task (Friedman's test, KF-WT group: Chi Sqr=5.08; p=0.07; KF-KO group: Chi Sqr=9.36; p=0.01) (**Fig.18**, panel E). Wilcoxon's test showed that KO group

put into action more Extended Searching than Finding (Z=2.02; p=0.04), and more Restricted Searching than Finding (Z=2.20; p=0.02).

Mann–Whitney's U test did not reveal significant differences between WT and KO groups in the Extended Searching (U=15.00; p=0.36), Restricted Searching (U=19.00; p=0.77) and Finding (U=9.00; p=0.07) strategies.

Both groups exhibited the same mean velocity (U=15.00; p=0.39) (**Fig.18**, panel G).

Males

Non-parametric analyses (Friedman's test) on Latencies revealed that both groups significantly reduced the times of platform finding as trials went by (WT: Chi Sqr=16.20; p=0.001; KO: Chi Sqr=12.77; p=0.005) (**Fig.18**, panel B). Mann–Whitney's U test did not reveal significant differences between KMWT and KMKO (trials 1-2: U=22.50; p=0.50; trials 3-4: U=15.00; p=0.13; trials 5-6: U=21.00; p=0.42; trials 7-8: U=18.00; p=0.25).

Friedman's test on Total Distance revealed that both groups significantly reduced the path to reach the platform as trials went by (WT group: Chi Sqr=16.20; p=0.001; KO group: Chi Sqr=11.74; p=0.008) (**Fig.18**, panel D). Mann–Whitney's U test did not reveal significant differences between WT and KO in the trials 1-2 (U=28.00; p=1.00), 3-4 (U=25.00; p=0.73), 5-6 (U=20.00; p=0.35), and 7-8 (U=22.00; p=0.49).

In WT and KO groups there were not significant differences among the Navigational Strategies used to perform the task (Friedman's test, WT group: Chi Sqr=3.71; p=0.15; KO group: Chi Sqr=3.62; p=0.16) (**Fig.18**, panel F). Mann–Whitney's U test did not reveal significant differences between WT and KO groups in the Extended Searching (U=22.50; p=0.52), Restricted Searching (U=23.00; p=0.55) and Finding (U=23.50; p=0.59) strategies.

Both groups exhibited the same mean velocity (U=27.00; p=0.91) (**Fig.18**, panel H).

Performances in the Place Phase

Females

However, Mann–Whitney's U test did not reveal significant differences between WT and KO in the first (U=20.50; p=0.94), second (U=10.00; p=0.12) and third (U=12.00; p=0.20) day of the MWM Place phase.

Friedman's test on Total Distance revealed that both groups significantly reduced the path to find the platform as the trials went by (WT group: Chi Sqr=10.28; p=0.005; KO group: Chi Sqr=7.00; p=0.03) (**Fig.19**, panel C). Furthermore, Mann–Whitney's U test did not reveal significant differences between WT and KO in the first (U=12.00; p=0.20), second (U=11.00; p=0.15) and third (U=19.00; p=0.77) day.

Only in WT group there was a significant difference among the Navigational Strategies used to perform the task (Friedman's test, WT group: Chi Sqr=6.00; p=0.05; KO group: Chi Sqr=2.17; p=0.33) (**Fig.19**, panel E). Wilcoxon's test showed that WT group put into action more Restricted Searching than Finding (Z=1.89; p=0.05). Mann–Whitney's U test did not reveal significant differences between WT and KO groups in the Extended Searching (U=13.50; p=0.27), Restricted Searching (U=15.00; p=0.38) and Finding (U=17.50; p=0.61) strategies. Both groups exhibited the same mean velocity (U=16.00; p=0.47) (**Fig.19**, panel G).

Males

Non-parametric analyses (Friedman's test) on Latencies revealed that both groups significantly reduced the times of platform finding as the trials went by (WT group: Chi Sqr=7.0; p=0.03; KO group: Chi Sqr=12.07; p=0.002) (**Fig.19**, panel B). Interestingly, while Mann–Whitney's U test did not reveal significant differences between WT and KO groups in the first (U=18.00; p=0.25) and third (U=28.00; p=1.00) day of the MWM Place phase, the groups were significantly different in the second day (U=4.00; p=0.005), indicating a slow-down in the learning shown by KO group.

Friedman's test on Total Distance revealed that both groups significantly reduced the path to find the platform as the trials went by (WT group: Chi Sqr=9.75; p=0.007; KO group: Chi Sqr=12.28; p=0.002) (**Fig.19**, panel D). Again, Mann–Whitney's U test did not reveal significant differences between WT and KO groups in the first (U=17.00; p=0.20) and third (U=26.00; p=0.81) day, but in the second (U=7.00; p=0.01) day of the task. This finding confirmed that the KO group showed a delayed learning.

Only in WT group there was a significant difference among the Navigational Strategies used (Friedman's test, WT group: Chi Sqr=12.45; p=0.001; KO group: Chi Sqr=3.71; p=0.14) (**Fig.19**, panel F). Wilcoxon's test showed that WT group put into action more Restricted Searching than Extended Searching and Finding (always Z=2.52; p=0.01). Mann–Whitney's U test did not reveal significant differences between WT and KO groups in the Extended Searching (U=17.00; p=0.20), Restricted Searching (U=13.50; p=0.09) and Finding (U=25.00; p=0.72) strategies.

Both groups swam at the same mean velocity (U=22.00; p=0.49) (**Fig.19**, panel H).

Probe Phase: Females and Males

WT and KO groups exhibited the same level of intact spatial memory performance both for females (U=17.00; p=0.57;Fig.13, panel A) and for males (U=24.00; p=0.64; **Fig.20**, panel B)

Summary

During the Cue Phase, when the escape platform emerged above the water level, both WT and KO (female and male) mice reached the platform more quickly and travelled less distances as trials went by, indicating the same good level of performance. However, the KO group put into action navigational strategies less direct to arrive on the platform.

During the Place Phase, when the escape platform was submerged under the water level, the KO group did not reduce the times of platform finding, even if both KO and WT groups travelled less distances as the trials went by. Furthermore, WT group put into action a navigational strategy targeted to search the platform only in some pool quadrants.

More importantly, even if both KO and WT groups reduced times and distances of platform finding as the trials went by, KO group showed a significantly delayed learning in comparison to WT group, that put into action a procedural navigational strategy more tuned to search the platform.

During the Probe Phase, both WT and KO (female and male) mice did not show any spatial memory deficits, given that the percentage of the total distance swum in the previously rewarded (platform) quadrant was higher than 25%.

The Rotarod performances

The Rotarod provides a way to test motor coordination or fatigue resistance in rodents.

As for females and males separately, the following Rotarod parameters were considered as indices: latency to fall (times); rotation speed when fall occurs; better latency to fall (time) showed by the animals in the last day of testing; better rotation speed showed by the animals in the last day of testing.

Females

Non-parametric analyses (Friedman's test) on times revealed that both groups significantly increased the latencies of falling as trials went by (WT: Chi Sqr=28.92; p=0.002; KO: Chi Sqr=28.49; p=0.003) (**Fig.21**, panel A). Mann–Whitney's U test did not reveal significant differences between WT and KO, but in trial 2 of day 3 (U=7.00; p=0.04) WT showed latencies higher than those exhibited by KO.

Similarly, Friedman's test on speed revealed that both groups significantly increased the velocity as trials went by (WT: Chi Sqr=25.25; p=0.008; KO: Chi Sqr=28.27; p=0.003) (**Fig.21**, panel C). Mann–Whitney's U test did not reveal significant differences between WT and KO, but in trial 2 of day 3 (U=7.00; p=0.04) WT showed velocity higher than that exhibited by KO.

Both groups showed the same better time (U=15.00; p=0.39, **Fig.21**, panel E) and better rotation speed (U=14.00; p=0.31, **Fig.21**, panel G) in the last day of testing.

Males

Non-parametric analyses (Friedman's test) on times revealed that both groups significantly increased the latencies of falling as trials went by (WT: Chi Sqr=19.47; p=0.05; KO: Chi Sqr=32.28; p=0.0007) (**Fig.21**, panel B). Mann–Whitney's U test did not reveal significant differences between WT and KO, but in trial 1 of day 1 (U=7.50; p=0.02) WT showed latencies higher than those exhibited by KO.

Similarly, Friedman's test on speed revealed that both groups significantly increased the velocity as trials went by (WT: Chi Sqr=19.41; p=0.05; KO: Chi Sqr=32.94; p=0.0005) (**Fig.21**, panel D). Mann–Whitney's U test did not reveal significant differences between WT and KO, but in trial 1 of day 1 (U=6.00; p=0.01) WT showed velocity higher than that exhibited by KO.

Both groups showed the same better time (U=25.00; p=0.73, **Fig.21**, panel F) and better rotation speed (U=26.50; p=0.86, **Fig.21**, panel H) in the last day of testing.

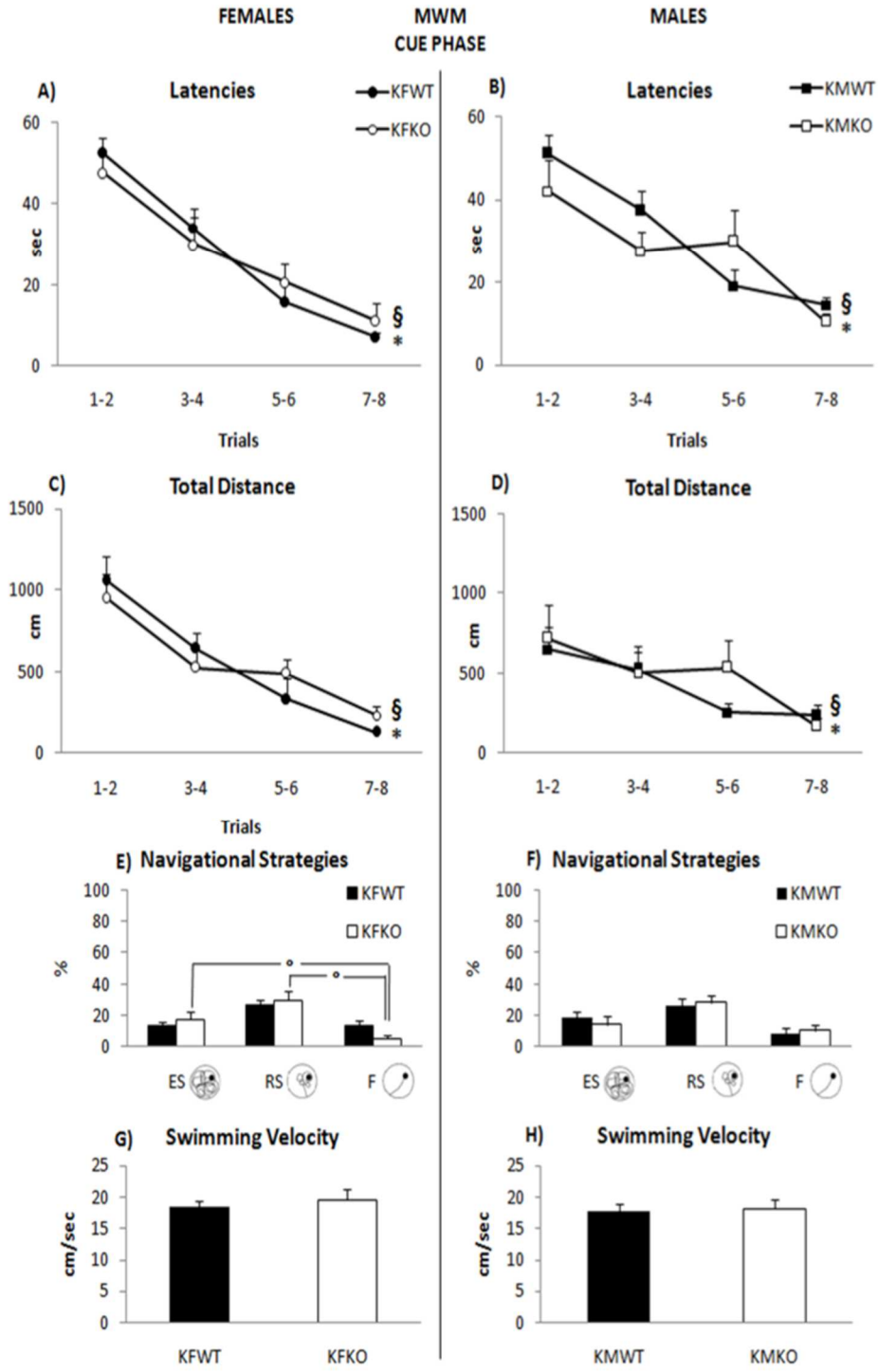

Fig.18 Behavioural observation in the KCASH2^{KO} mice: The Cue Phase
Results of Cue Phase of MWM test. The average the time of latency to find the platform as the trials (A-B), the total distance (C-D), the navigational strategies (E-F) and the swim speed (G-H) are shown. Analyses show a different navigational strategy in KFKO group (female KCASH2^{KO}) respect to KFWT group (female WT). The different navigational strategies are depicted under the graphs. ES: Extended Searching; RS: Restricted Searching; F: Finding.

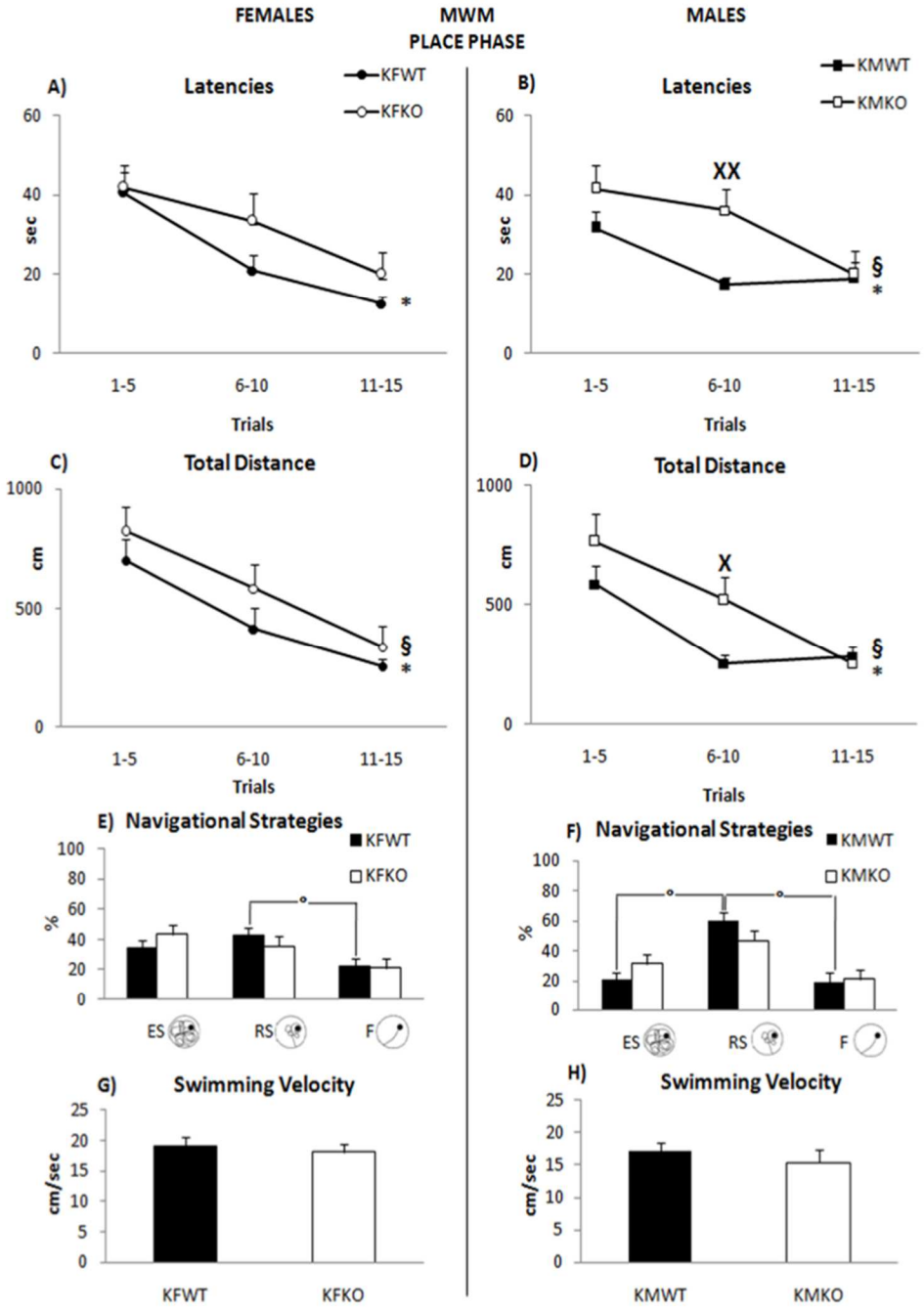

Fig.19 Behavioural observation in the KCASH2^{KO} mice: The Place Phase.
Results of Place Phase of MWM test. Analyses show Analyses show more Restricted Searching (RS) than Finding in KFKO group (female KCASH2^{KO}) respect to KFWT group (female WT). While the KMKO group (male KCASH2^{KO}) shows a slow-down learning respect to KMWT (male WT).

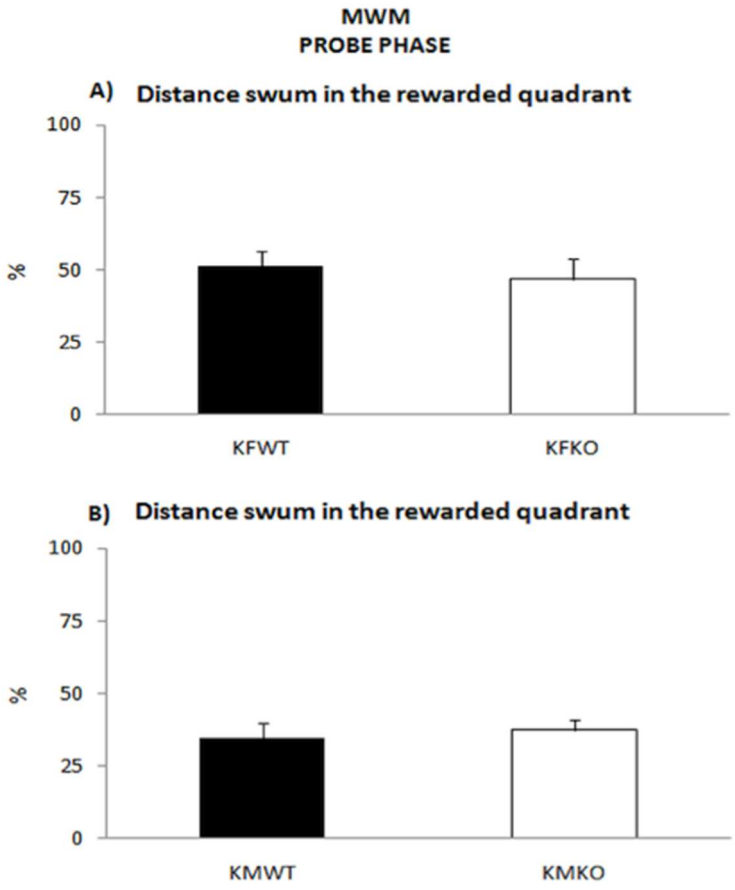

Fig.20 Behavioural observation in the KCASH2^{KO} mice: The Probe Phase. Results of Probe Phase of MWM test exhibited the same level of intact spatial memory performance between the both group (KFKO/KMKO) compared to WT mice.

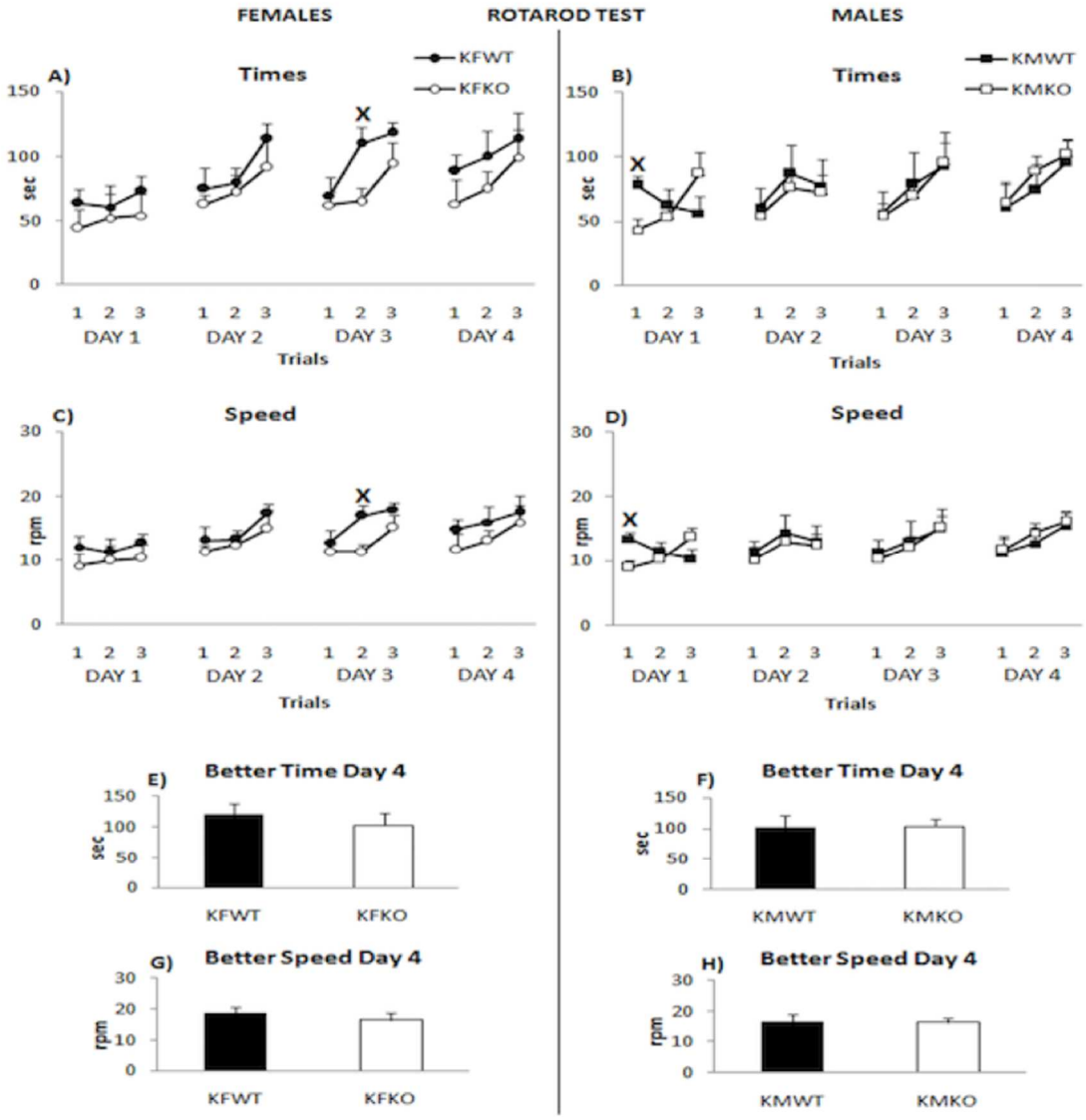

Fig.21. **Motor balance test: the Rotarod Test**
Motor balance in the Rotarod test shows no significant difference between both group (KFKO/KMKO) compared to WT mice.

Additional KCASH2 dependent phenotypes

In the search for additional tissues in which KCASH2 may play a role, we screened other organs and tissues obtained from $KCASH2^{KO}$ mice (and relative WT controls) for β-gal activity.

Since the literature had been reported potential endogenous β-gal activity in WT mice, we adapted the β-gal assay in order to strongly reduce β-gal endogenous activity (see methods) (**Fig.22**, panel A), and then performed the assay on different tissues.

Interestingly, we found β-gal activity in $KCASH2^{KO}$ testis and epididymis, while the control WT tissues did not present β-gal staining.

Analysis of protein extracts from testis and epididymis by western blot, confirmed the expression of KCASH2 protein in normal WT mice (**Fig.22**, panel B).

The reporter gene expression in $KCASH2^{KO}$ mice reveals β-gal protein in Leydig cells of testis (**Fig.22**, panel C) and in the epididymal epithelium with a gradient pattern from caput to cauda (**Fig.22**, panel D). The caput, corpus and cauda epididymis in mice are organized into a series of intra-regional segments and we observed a more intense staining at 3-4-5-7-8-9-10 epididymal segments level. (**Fig.22**, panel D).

The Hh signalling pathway has been involved in development of testis and epididymis and function (Szczepny et al., 2009). In particular Desert Hh (Dhh) is secreted from Sertoli cells (Szczepny et al., 2006) and modulates development and differentiation of Leydig cells (Yao et al., 2002). Consequently *Dhh*-null males display peritubular cell abnormalities and severely impaired spermatogenesis (Bitgood et al., 1996). While Sonic Hh is expressed in the epididymis and is involve to the sperm motility (Turner et al., 2006).

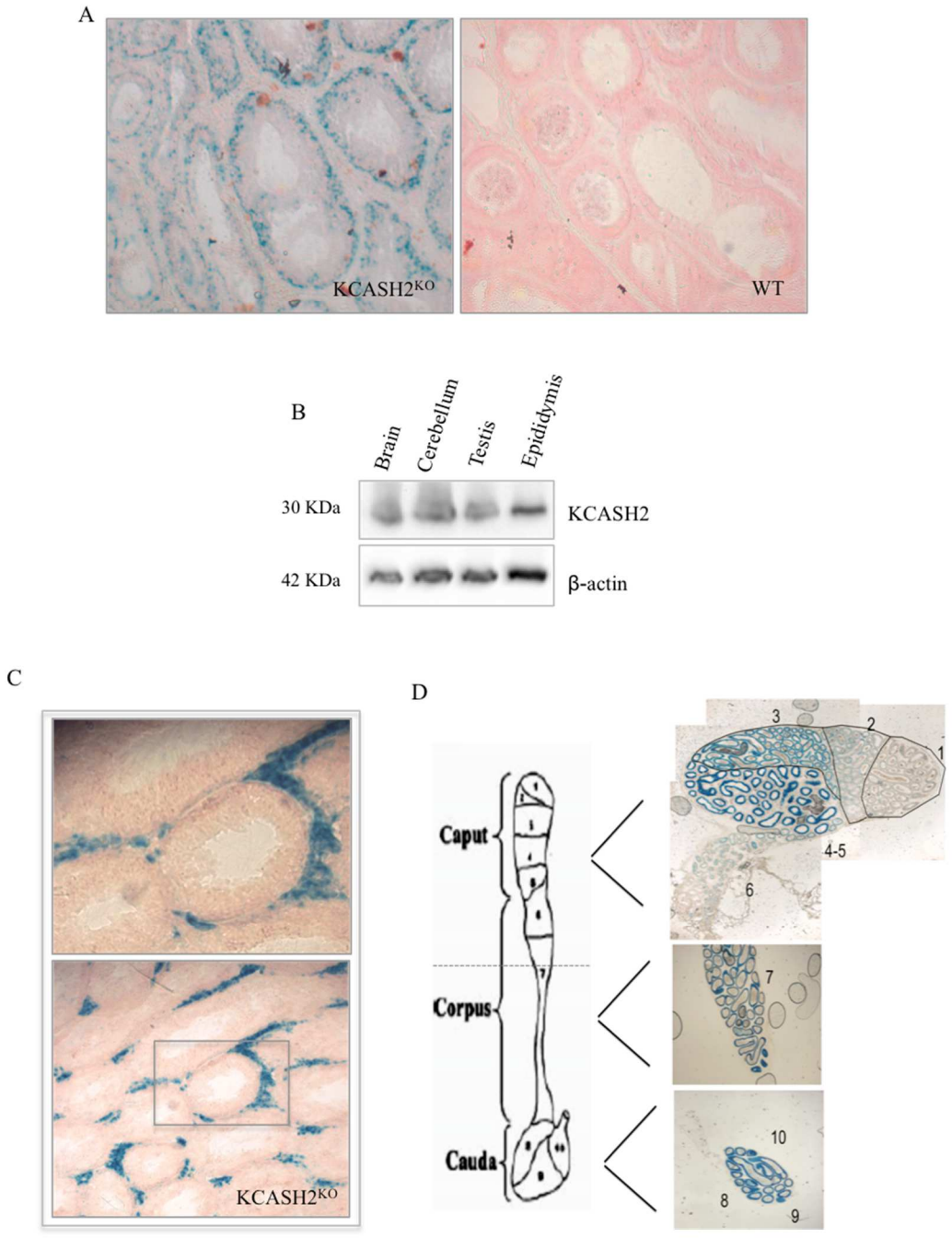

Fig.22 KCASH2 expression in Testis and Epididymis.

(A) Setting βGal assay. (B) Western Blot of KCASH2 in the testis and epididymis of Adult KCASH2^{KO} and WT mice. The reporter gene expression in KCASH2-KO mice reveals cellular localization in Testis Leydig cells (C) and in the epididymal epithelium with a pattern caput-cauda (D).

Altered Spermatozoa morphology and motility in KCAH2^{KO} mice

To investigate if KCASH2 has a physiological role in spermatozoa generation and maturation, we conduced both a morphological analysis and motility test in sperm sample collected from the WT and KCASH2^{KO} mice.

In collaboration with laboratory of Prof. Lucio Gnessi, we conducted microscopic observation of sperm suspension. Sperm counts, morphology and motility were evaluated using a cell counting chamber under light microscope.

We observed significant anomalies in KCASH2^{KO} mice spermatozoa; in particular there was a significant increase of atypical elements, with a corresponding reduction of typical elements. Interestingly the number of acephalic elements increased dramatically (more than doubled) (**Fig.23**, panel A).

Furthermore, spermatozoa analysis presented a reduction of the number of spermatozoa with rectilinear fast motility, and an increase of dyskinetic spermatozoa (**Fig.23**, panel B).

In summary, KCASH2^{KO} mice present a significant reduction of fertile spermatozoa. This reduction does not lead to total infertility since the mice are still able to reproduce.

So far, a more quantitative analysis of the breeding outcome from WT and KCASH2^{KO} mice is ongoing. We will set up several breeding pair and monitor the number of pups and the success rate of each breeding.

A

SPERMATOZOA MORPHOLOGICAL DATA					
		WT (n=8)		Kcash2 KO (n=8)	
		Average	st.dev.	Average	st.dev.
Typical elements	%	21,9	*10,3*	8.1**	*6,5*
Atypical elements	%	**78,1**	*10,3*	**91.9****	*6,5*
- cytoplasmic residues	%	13,8	*3,5*	12,5	*3,8*
- angulated necks	%	13,1	*7,0*	21,3	*9,2*
- heads pointed	%	13,8	*6,4*	13,1	*3,7*
- acephalic	%	**5,0**	*2,7*	**12.5****	*3,8*
- microcephalic	%	13,8	*6,4*	12,5	*2,7*
- macrocephalic	%	7,8	*5,7*	7,5	*3,8*
- ball heads	%	7,5	*2,7*	7,5	*4,6*
- rolled tails	%	2,3	*2,5*	5,0	*7,1*
SPERMATOZOA/ml		20.862.500	*4.248.697*	21.906.875	*5.059.978*
SPERMATOZOA/mg epididymis		171.333	*109.023*	201.316	*163.866*

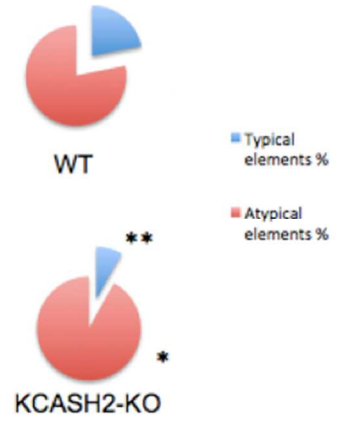

B

MOTILITY ANALYSIS					
		Ctrls (n=8)		Kcash2 KO (n=8)	
		Average	st.dev.	Average	st.dev.
Total motility	%	63,3	*12,4*	62,5	*14,5*
total rectilinear	%	**40,8**	*22,7*	**15.8***	*15,1*
- fast	%	**13,3**	*8,0*	**2.5****	*3,7*
- slow	%	27,5	*16,0*	13,3	*12,0*
Agitational in loco	%	5,8	*2,3*	10,0	*9,2*
Dyskinesia	%	**16,7**	*13,4*	**36.7***	*18,9*

*p< 0.05 **p < 0.01

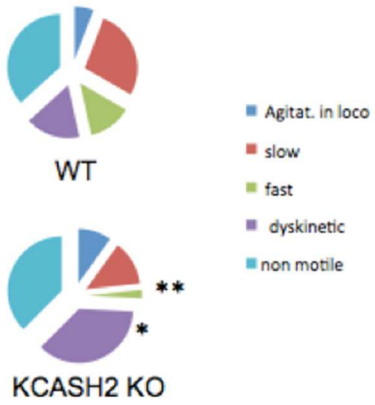

Fig.23 Altered Spermatozoa Morphology and Motility in KCASH2^{KO} mice.

(A) Morphological analysis of spermatozoa collected from the WT and KCASH2^{KO} mice, by microscopic observation of sperm suspension, show that in KCASH2^{KO} mice spermatozoa, such as presence of significant atypical elements (acephalic). (B) Evaluation of the motility reveals an increased dyskinesia in KCASH2^{KO} spermatozoa. Data are presented as mean and standard deviation; student's t-test was used for statistical analysis and P<0.05 (*) was considered statistically significant; ** indicates p<0.001.

DISCUSSION

Our Previous studies have demonstrated that KCASH2 is a negative regulator of Shh signaling, and its expression is downregulated in most human MB.

In the present work, we generated a KCASH2 knockout mice ($KCASH2^{KO}$) to evaluate the in vivo effect of KCASH2 deletion on the Shh pathway and cerebellar development.

This mouse model has a LacZ cassette inserted 5' of the KCASH2 gene, whose expression is modulated by the KCASH2 endogenous promoter and therefore is a good model to visualize KCASH2 expression by β-Gal assay on different tissues at different developmental stages.

As expected, β-Gal activity was present in differentiating and differentiated cerebellar granule cells. Given the critical role of the Shh pathway in GCP development, we hypothesized that KCASH2 loss could affect this process.

Although we could not observe a gross phenotype, a more accurate analysis highlighted a larger thickness of the IGL. In particular, the IV-V cerebellar lobules in the adult $KCASH2^{KO}$ mice cerebellum presented a significant increase (close to 15%) in the IGL compared to the WT mice.

These data are consistent with a mild Shh-dependent phenotype previously described in the Shh-P1 mouse model (Corrales et al. 2004), which presents transgenic expression of a Shh construct, containing part of the Shh promoter (Riccomagno et al, 2002). The Shh-P1 mouse model, presents a mildly enlarged cerebellum, in particular in correspondence of III, IV, V and IX lobules, due to over proliferation of granule cells (Corrales et al., 2004). Consistently, our results revealed an increased proliferation of GCPs in the $KCASH2^{KO}$ cerebella. This proliferation correlated with a significant increase of Gli1 protein levels in

the EGL, indicating the persistence of an elevated Hh signaling, which determined a prolonged proliferation of granule cell precursors.

Previous studies have shown that in WT mice P5-6 is the time of maximal EGL GCPs proliferation, while the number of proliferating GCPs in the EGL begin to decrease at P7, until few proliferating cells remain in the EGL at P14 (Wu et al, 2012).

As expected in the KCASH2^{KO} mice the numbers of proliferating, Ki67-positive cells are significantly more elevated from P7 to at least P10. However, after P10 the difference between WT and KCASH2^{KO} EGL proliferation decreases gradually, and by P16 almost all the EGL is differentiated in both mice. This phenomenon may be explained by the fact that GCP may be able to compensate for KCASH2 loss and ultimately differentiate. A first hypothesis to explain this effect is that the Hh signal may be ultimately turned off by reduction of Shh secretion by Purkinje cell, so that the downstream regulation by KCASH2 becomes less relevant. This Hypothesis is probably in contrast with the observation by Lewis and colleagues that Purkinje cells express Shh up to the adult age (Lewis et al., 2004). A second hypothesis is that GCP may compensate for KCASH2 loss thanks to the presence of other members of KCASH family, in particular KCASH1, which is able to induce HDAC1 ubiquitination and its proteasomal degradation trough the same mechanism of KCASH2. This second hypothesis is supported by our observations that KCASH1 expression is significantly enhanced (more than doubled starting from P21 up to P28) in KCASH2^{KO} cerebella.

Our previous studies indicated that KCASH2 is a tumour suppressor gene which is deleted or silenced in Hh-dependent Medulloblastoma, the most common malignant cerebellar tumour. MB tumorigenesis generally is associated to an increase of cellular proliferation that ultimately leads to accumulation of tumorigenetic mutations (Wu et al, 2012). For this reason, we looked for evidences of MB formation in KO mice. At the moment, although

the number of animals analysed is small (4 KO mice), and the time of observation is limited to 1 year, we could not find evidences of tumours.

Even though we cannot exclude the possibility that an increase in the number of animals and of the time of the observation may unveil the presence of tumorigenic events, the absence of MB formation would not be completely surprising. First, we have seen that GCP are able to partially compensate for the loss of KCASH2. Second, several groups have demonstrated that the presence of a single oncosuppressor's mutation may not be sufficient for the transformation of cells. For example, almost 100% Ptch heterozygous mice present areas of hyperproliferative GCP, in the early development; but only 15% of these mice develop MB in the adulthood (Goodrich et al 1997).

Although KCASH2 deficiency did not promote tumorigenesis in the cerebellum, we suggest that KCASH2^{KO} mice may provide a mouse model to study KCASH2 loss as a risk factor for MB tumorigenesis. Previous works have already shown as increase the incidence of Medulloblastoma development in double mutant murine models. For example, in Ptch+/-/Kip1 and Ptch+/-/Hic1+/- mice models there is an increased MB incidence from 40% to 60%. Indeed, in Ptch+/-/Tp53 mice model the incidence of MB was 93%.

According to these data, we are planning to generate a double mutant Ptch+/-/KCASH2^{KO} mouse to verify if KCASH2 can increase the incidence of MB development compared to Ptch+/- mice.

During our β-Gal assays on KCASH2^{KO} brain sections, we unexpectedly detected β-Gal also in Purkinje cells, starting from day 7 postnatal (P7) until adulthood. This result is partially unexpected, since Purkinje cells (which secrete Shh) have been described to express Gli1 starting from P5 to adulthood (Corrales et al 2004), and similarly Ptch1 (Lewis et al 2004) thus implying an active hedgehog pathway.

The presence of Gli1 expression in Purkinje cells implies that in this context KCASH2 may have a mild inhibitory effect or be expressed physiologically at low levels. In the context

of a KCASH2^{KO} mouse, the activation of KCASH2 promoter does not lead to the production of KCASH2 protein, but only to translation of beta gal protein. The absence of KCASH2 function may in turn push the cells to further induce transcription from the KCASH2 promoter, leading to a dramatic increase of b-gal protein in the cells.

As a consequence, Purkinje cells may present a constitutive high expression of β-Gal in the failed attempt to finely regulate the Shh pathway activity. This hypothesis would imply that in KCASH2^{KO} mouse, the Purkinje cells may be more responsive to the Shh pathway, in an autocrine mechanism, producing higher levels of Gli1 and Ptch mRNA. Unfortunately, probably for technical difficulties with the antibodies, we have not been able to compare the presence of Gli1 or Ptch1 protein in WT and KCASH2^{KO} Purkinje cells. On the other end, we have been able to monitor the levels of HDAC1 protein. As expected, while the WT Purkinje do not express HDAC1 protein, in KCASH2^{KO} mice, Purkinje cells express high levels of HDAC1, implying that in this context Gli1 protein may be deacetylated and fully active.

Previous works have demonstrated that HDACs inhibitors, as valproic acid and sodium butyrate, block the differentiation of neuronal precursor, indicating that these proteins play an important role in CNS development and neural progenitor proliferation and differentiation (Laeng et al., 2004).

These observations make us assume that loss of KCASH2 and overexpression of HDAC1 may have a pathological effect on Purkinje cells morphology and functionality, that will need further investigation, looking at both cell morphology and electrophysiology.

β-Gal activity has been detected not only in cerebellum but also in cerebral cortex and hippocampus. These results make us wonder if KCASH2 can be associated with cerebellar or hyppocampal cognitive function.

The results of MWM tests have highlighted a significant alteration in functions that may be reconducted to cerebellum, while hippocampal functions appear to be less affected.

Indeed, the loss of KCASH2 induces in male KCASH2^{KO} a delayed learning and in female KCASH2^{KO} a diversity in procedural navigational strategy compared to WT siblings.

Our observations are the first to suggest a role of the Hh pathway alteration in such behavioural disorders related to cerebellar function.

It has to be noted that recently Zanin et al. have proposed that reduction of HDAC1 protein (induced by loss of p75^{NTR}) in GCPs may lead to deficits in motor/balance coordination functions, as assessed by the Rotarod test (Zanin et al., 2016).

On the other end, the results obtained by us on the Rotarod test do not highlight significative differences in the KCASH2^{KO} mouse, indicating that the model used by Zanin et al may present additional alterations (HDAC1-independent, such as NF-kB pathway, cyclin E, B, JNK, caspases etc) due to the loss of the p75^{NTR}.

We are currently planning to explore several other tests in order to unveil potential alterations in hyppocampal functions.

During the characterization of the KCASH2^{KO} mouse, we unveiled a potential physiological role of KCASH2 in spermatozoa development and function. This function may be mediated by the action of KCASH2 on the sonic hedgehog pathway.

In fact, Dhh ligand is produced in the testis, specifically in Sertoli cells, where it plays a role in germ cell development (Bitgood et al, 1996; Kroft et al, 2001). At the same time Shh expression has been detected in the adult epididymis, where is present a gradient of expression from the caput to the cauda (Turner et al., 2004).

We have demonstrated that KCASH2 is expressed in Leydig cells and in epididymal epithelium cells and we have observed anomalies in KCASH2^{KO} mice spermatozoa morphology (increased atipicity) and sperm mobility (dyskinesia). While the results have important potential implications, so far, we do not have identified the molecular mechanism

that underlies these alterations. We could not detect gross alterations in size and morphology of testis and epididymis, and the total count of the spermatozoa is not significantly altered.

Literature date indicate that during passage through the epididymis, the spermatozoa undergo various morphological and functional changes that result in their competence for fertilization (Bedford 1975; Cooper 1995). These include the ability to move, to undergo the acrosome reaction, and to penetrate the zona pellucida. In addition, a high percentage of male infertility in humans was suggested to originate in the alteration of the epididymal environment (Lunde et al. 1990). However, our observations seem to imply further alteration, since the mice are fertile (although we cannot exclude a reduction in fertility), and present alterations in spermatozoa morphology and motility. It has to be noted that Shh pathway inhibition has been demonstrated to alter epididymal function as assessed by the development of sperm motility (Turner et al., 2006).

Further extensive research will be needed to better understand the mechanism through which KCASH2 affects spermatogenesis. As a first step it will be necessary to verify the modulation of the different components of the Hh pathway in KCASH2^{KO} tissues (testis and epididymis) compared with WT samples, during the developmental and differentiation steps. We also plan to perform a high throughput screening to identify potential other KCASH2 targets.

REFERENCES

- Aberger F, Kern D, Greil R, Hartmann TN. *Canonical and non-canonical Hedgehog/GLI signaling in haematological malignancies*. Vitam Horm. 2012; 88:25-54.
- Álvarez-Buylla A, Ihrie RA. *Sonic hedgehog signaling in the postnatal brain.* Semin Cell Dev Biol. 2014 Sep; 33:105-11.
- Argenti B, Gallo R, Di Marcotullio L, Ferretti E, Napolitano M, Canterini S, De Smaele E, Greco A, Fiorenza MT, Maroder M, Screpanti I, Alesse E, Gulino A. *Hedgehog antagonist REN(KCTD11) regulates proliferation and apoptosis of developing granule cell progenitors*. J Neurosci. 2005 Sep 7; 25(36):8338-46.
- Barakat MT, Humke EW, Scott MP. *Kif3a is necessary for initiation and maintenance of medulloblastoma.* Carcinogenesis. 2013 Jun;34(6):1382-92.
- Behesti H, Marino S. *Cerebellar granule cells: insights into proliferation, differentiation, and role in medulloblastoma pathogenesis.* Int J Biochem Cell Biol. 2009 Mar; 41(3):435-45.
- Belgacem YH, Borodinsky LN. *Inversion of Sonic hedgehog action on its canonical pathway by electrical activity*. Proc Natl Acad Sci U S A. 2015 Mar 31; 112(13):4140-5.
- Berndsen CE, Wolberger C. *New insights into ubiquitin E3 ligase mechanism.* Nat Struct Mol Biol. 2014 Apr; 21(4):301-7.
- Bihannic L, Ayrault O. *Insights into cerebellar development and medulloblastoma.* Bull Cancer. 2016 Jan; 103(1):30-40.
- Bitgood MJ, Shen L, McMahon AP. *Sertoli cell signaling by desert hedgehog regulates the male germline*. Curr Biol 1996; 6: 298 304
- Butts T, Green MJ, Wingate RJ. *Development of the cerebellum: simple steps to make a 'little brain'*. Development. 2014 Nov;141(21):4031-41.

- Canettieri G, Di Marcotullio L, Greco A, Coni S, Antonucci L, Infante P, Pietrosanti L, De Smaele E, Ferretti E, Miele E, Pelloni M, De Simone G, Pedone EM, Gallinari P, Giorgi A, Steinkühler C, Vitagliano L, Pedone C, Schinin ME, Screpanti I, Gulino A. *Histone deacetylase and Cullin3-REN(KCTD11) ubiquitin ligase interplay regulates Hedgehog signalling through Gli acetylation*. Nat Cell Biol. 2010 Feb; 12(2):132-42.
- Carballo GB, Honorato JR, de Lopes GPF, Spohr TCLSE. *A highlight on Sonic hedgehog pathway*. Cell Commun Signal. 2018 Mar 20; 16(1):11.
- Carletti B, Rossi F. *Neurogenesis in the cerebellum.* Neuroscientist. 2008 Feb; 14(1):91-100.
- Cheng Y, Sudarov A, Szulc KU, Sgaier SK, Stephen D, Turnbull DH, Joyner AL. *The Engrailed homeobox genes determine the different foliation patterns in the vermis and hemispheres of the mammalian cerebellum.* Development. 2010 Feb; 137(3):519-29.
- Choi JH, Kwon HJ, Yoon BI, Kim JH, Han SU, Joo HJ, Kim DY. *Expression profile of histone deacetylase 1 in gastric cancer tissues*. Jpn J Cancer Res. 2001 Dec; 92(12):1300-4.
- Cogen PH, McDonald JD. Tumor suppressor genes and medulloblastoma. J Neurooncol. 1996 Jul; 29(1):103-12.
- Cohen MM Jr. *The hedgehog signaling network.* Am J Med Genet A. 2003 Nov 15; 123A (1):5-28.
- Coni S, Antonucci L, D'Amico D, Di Magno L, Infante P, De Smaele E, Giannini G, Di Marcotullio L, Screpanti I, Gulino A, Canettieri G. *Gli2 acetylation at lysine 757 regulates hedgehog-dependent transcriptional output by preventing its promoter occupancy*. PLoS One. 2013 Jun

- Corrales JD, Rocco GL, Blaess S, Guo Q, Joyner AL. *Spatial pattern of sonic hedgehog signaling through Gli genes during cerebellum development*. Development. 2004 Nov; 131(22):5581-90. Epub 2004 Oct 20.
- Correale S, Pirone L, Di Marcotullio L, De Smaele E, Greco A, Mazzà D, Moretti M, Alterio V, Vitagliano L, Di Gaetano S, Gulino A, Pedone EM. *Molecular organization of the cullin E3 ligase adaptor KCTD11*. Biochimie. 2011 Apr; 93(4):715-24.
- Dahmane N, Ruiz i Altaba A. *Sonic hedgehog regulates the growth and patterning of the cerebellum*. Development. 1999 Jun;126 (14):3089-100
- De Luca A, Cerrato V, Fucà E, Parmigiani E, Buffo A, Leto K. *Sonic hedgehog patterning during cerebellar development*. Cell Mol Life Sci. 2016 Jan; 73(2):291-303.
- De Smaele E, Di Marcotullio L, Ferretti E, Screpanti I, Alesse E, Gulino A. Chromosome 17p deletion in human medulloblastoma: a missing checkpoint in the Hedgehog pathway. Cell Cycle. 2004 Oct; 3(10):1263-6.
- De Smaele E, Di Marcotullio L, Moretti M, Pelloni M, Occhione MA, Infante P, Cucchi D, Greco A, Pietrosanti L, Todorovic J, Coni S, Canettieri G, Ferretti E, Bei R, Maroder M, Screpanti I, Gulino A. *Identification and characterization of KCASH2 and KCASH3, 2 novel Cullin3 adaptors suppressing histone deacetylase and Hedgehog activity in medulloblastoma*. Neoplasia. 2011 Apr; 13(4):374-85.
- Di Marcotullio L, Ferretti E, De Smaele E, Argenti B, Mincione C, Zazzeroni F, Gallo R, Masuelli L, Napolitano M, Maroder M, Modesti A, Giangaspero F, Screpanti I, Alesse E, Gulino A. *REN(KCTD11) is a suppressor of Hedgehog signaling and is deleted in human medulloblastoma*. Proc Natl Acad Sci U S A. 2004 Jul 20; 101(29):10833-8.
- Di Marcotullio L, Ferretti E, Greco A, De Smaele E, Screpanti I, Gulino A. *Multiple ubiquitin-dependent processing pathways regulate hedgehog/gli signaling:*

implications for cell development and tumorigenesis. Cell Cycle. 2007 Feb 15; 6(4):390-3.

- Di Marcotullio L, Greco A, Mazzà D, Canettieri G, Pietrosanti L, Infante P, Coni S, Moretti M, De Smaele E, Ferretti E, Screpanti I, Gulino A. *Numb activates the E3 ligase Itch to control Gli1 function through a novel degradation signal*. Oncogene. 2011 Jan 6; 30(1):65-76.
- Eguether T, Hahne M. *Mixed signals from the cell's antennae: primary cilia in cancer.* EMBO Rep. 2018 Oct 22. pii: e46589. Review.
- Faryna M, Konermann C, Aulmann S, Bermejo JL, Brugger M, Diederichs S, Rom J, Weichenhan D, Claus R, Rehli M, Schirmacher P, Sinn HP, Plass C, Gerhauser C. *Genome-wide methylation screen in low-grade breast cancer identifies novel epigenetically altered genes as potential biomarkers for tumor diagnosis*. FASEB J. 2012 Dec; 26(12):4937-50.
- Federico F, Leggio MG, Neri P, Mandolesi L, Petrosini L. *NMDA receptor activity in learning spatial procedural strategies II. The influence of cerebellar lesions*. Brain Res Bull. 2006, 70 (4–6): 356-367.
- Ferretti E, De Smaele E, Di Marcotullio L, Screpanti I, Gulino A. *Hedgehog checkpoints in medulloblastoma: the chromosome 17p deletion paradigm.* Trends Mol Med. 2005 Dec; 11(12):537-45.
- Fleming JT, He W, Hao C, Ketova T, Pan FC, Wright CC, Litingtung Y, Chiang C. *The Purkinje neuron acts as a central regulator of spatially and functionally distinct cerebellar precursors*. Dev Cell. 2013 Nov 11; 27(3):278-92.
- Foti F, Laricchiuta D, Cutuli D. *Exposure to an enriched environment accelerates recovery from cerebellar lesion*. Cerebellum. 2011, 10 (1): 104-119.
- Fuccillo M, Joyner AL, Fishell G. *Morphogen to mitogen: the multiple roles of hedgehog signalling in vertebrate neural development*. Nat Rev Neurosci. 2006 Oct; 7(10):772-83.

- Gallo R, Zazzeroni F, Alesse E, Mincione C, Borello U, Buanne P, D'Eugenio R, Mackay AR, Argenti B, Gradini R, Russo MA, Maroder M, Cossu G, Frati L, Screpanti I, Gulino A. *REN: a novel, developmentally regulated gene that promotes neural cell differentiation*. J Cell Biol. 2002 Aug 19;158(4):731-40.
- Gandhi CC, Kelly RM, Wiley RG, Walsh TJ. *Impaired acquisition of a Morris water maze task following selective destruction of cerebellar purkinje cells with OX7-saporin*. Behav Brain Res. 2000, 109 (1): 37-47.
- Gilder AS, Chen YB, Jackson RJ 3rd, Jiang J, Maher JF. *Fem1b promotes ubiquitylation and suppresses transcriptional activity of Gli1*. Biochem Biophys Res Commun. 2013 Oct 25;440(3):431-6.
- Goodrich LV, Milenković L, Higgins KM, Scott MP. *Altered neural cell fates and medulloblastoma in mouse patched mutants*. Science. 1997 Aug 22; 277(5329):1109-13.
- Guerrini-Rousseau L, Dufour C, Varlet P, Masliah-Planchon J, Bourdeaut F, Guillaud-Bataille M, Abbas R, Bertozzi AI, Fouyssac F, Huybrechts S, Puget S,Bressac-De Paillerets B, Caron O, Sevenet N, Dimaria M, Villebasse S, Delattre O, Valteau-Couanet D, Grill J, Brugières L. *Germline SUFU mutation carriers and medulloblastoma: clinical characteristics, cancer risk, and prognosis*. Neuro Oncol. 2018 Jul 5;20(8):1122-1132.
- Gulino A, Di Marcotullio L, Canettieri G, De Smaele E, Screpanti I. *Hedgehog/Gli control by ubiquitination/acetylation interplay*. Vitam Horm. 2012; 88:211-27.
- Halkidou K, Gaughan L, Cook S, Leung HY, Neal DE, Robson CN. *Upregulation and nuclear recruitment of HDAC1 in hormone refractory prostate cancer*. Prostate. 2004 May 1; 59(2):177-89.
- Hahn H (1), Wojnowski L, Zimmer AM, Hall J, Miller G, Zimmer A. *Rhabdomyosarcomas and radiation hypersensitivity in a mouse model of Gorlin syndrome*. Nat Med. 1998 May;4(5):619-22.

- Hallahan AR, Pritchard JI, Hansen S, Benson M, Stoeck J, Hatton BA, Russell TL, Ellenbogen RG, Bernstein ID, Beachy PA, Olson JM. *The SmoA1 mouse model reveals that notch signaling is critical for the growth and survival of sonic hedgehog-induced medulloblastomas*. Cancer Res. 2004 Nov 1; 64(21):7794-800.
- Heshmati M, Russo SJ. *Learning to deal with life's ups and downs*. Nat Neurosci. 2013 Jun;16(6):658-9.
- Hoshino M, Nakamura S, Mori K, Kawauchi T, Terao M, Nishimura YV, Fukuda A, Fuse T, Matsuo N, Sone M, Watanabe M, Bito H, Terashima T, Wright CV, Kawaguchi Y, Nakao K, Nabeshima Y. *Ptf1a, a bHLH transcriptional gene, defines GABAergic neuronal fates in cerebellum*. Neuron. 2005 Jul 21; 47(2):201-13.
- Huang S, Zhang Z, Zhang C, Lv X, Zheng X, Chen Z, Sun L, Wang H, Zhu Y, Zhang J, Yang S, Lu Y, Sun Q, Tao Y, Liu F, Zhao Y, Chen D. *Activation of Smurf E3 ligase promoted by smoothened regulates hedgehog signaling through targeting patched turnover*. PLoS Biol. 2013 Nov;11(11): e1001721.
- Huang X, Ketova T, Fleming JT, Wang H, Dey SK, Litingtung Y, Chiang C. *Sonic hedgehog signaling regulates a novel epithelial progenitor domain of the hindbrain choroid plexus*. Development. 2009 Aug; 136(15):2535-43.
- Huang X, Liu J, Ketova T, Fleming JT, Grover VK, Cooper MK, Litingtung Y, Chiang C. *Transventricular delivery of Sonic hedgehog is essential to cerebellar ventricular zone development*. Proc Natl Acad Sci U S A. 2010 May 4; 107(18):8422-7.
- Huangfu D, Anderson KV. *Cilia and Hedgehog responsiveness in the mouse*. Proc Natl Acad Sci U S A. 2005 Aug 9;102(32):11325-30.
- Infante P, Faedda R, Bernardi F, Bufalieri F, Lospinoso Severini L, Alfonsi R, Mazzà D, Siler M, Coni S, Po A, Petroni M, Ferretti E, Mori M, De Smaele E, Canettieri G, Capalbo C, Maroder M, Screpanti I, Kool M, Pfister SM, Guardavaccaro D, Gulino A, Di

Marcotullio L. *Itch/β-arrestin2-dependent non-proteolytic ubiquitylation of SuFu controls Hedgehog signalling and medulloblastoma tumorigenesis.* Nat Commun. 2018 Mar 7; 9(1):976.

- Ingham PW. How cholesterol modulates the signal. Curr Biol. 2000 Mar 9;10(5): R180-3. Review.
- Kawahira H, Ma NH, Tzanakakis ES, McMahon AP, Chuang PT, Hebrok M. *Combined activities of hedgehog signaling inhibitors regulate pancreas development.* Development. 2003 Oct; 130(20):4871-9.
- Kipnis J, Gadani S, Derecki NC. *Pro-cognitive properties of T cells*. Nat Rev Immunol. 2012 Sep;12(9):663-9. Epub 2012 Aug 20. Review.
- Koehler DR, Downey GP, Sweezey NB, Tanswell AK, Hu J. *Lung inflammation as a therapeutic target in cystic fibrosis*. Am J Respir Cell Mol Biol. 2004 Oct; 31(4):377-81.
- Kroft TL, Patterson J, Won Yoon J, Doglio L, Walterhouse DO, Iannaccone PM, Goldberg E. *GLI1 localization in the germinal epithelial cells alternates between cytoplasm and nucleus: upregulation in transgenic mice blocks spermatogenesis in pachytene.* Biol Reprod. 2001 Dec;65(6):1663-71.
- Lackey EP, Heck DH, Sillitoe RV. *Recent advances in understanding the mechanisms of cerebellar granule cell development and function and their contribution to behavior.* F1000Res. 2018 Jul 26;7. pii: F1000 Faculty Rev-1142.
- Laeng P, Pitts RL, Lemire AL, Drabik CE, Weiner A, Tang H, Thyagarajan R, Mallon BS, Altar CA. *The mood stabilizer valproic acid stimulates GABA neurogenesis from rat forebrain stem cells.* J Neurochem. 2004 Oct;91(1):238-51.
- Laricchiuta D, Cavallucci V, Cutuli D, De Bartolo P, Caporali P, Foti F, Finke C, D'Amelio M, Manto M, Petrosini L. *Effects of Anti-NMDA Antibodies on Functional Recovery and Synaptic Rearrangement Following Hemicerebellectomy*. Neuromolecular Med. 2016, 18(2): 190-202.

- Leggio MG, Neri P, Graziano A. *Cerebellar contribution to spatial event processing: characterization of procedural learning*. Exp Brain Res. 1999, 127 (1): 1-11.
- Legué E, Gottshall JL, Jaumouillé E, Roselló-Díez A, Shi W, Barraza LH, Washington S, Grant RL, Joyner AL. *Differential timing of granule cell production during cerebellum development underlies generation of the foliation pattern*. Neural Dev. 2016 Sep 8; 11(1):17.
- Leto K, Arancillo M, Becker EB, Buffo A, Chiang C, Ding B, Dobyns WB, Dusart I, Haldipur P, Hatten ME, Hoshino M, Joyner AL, Kano M, Kilpatrick DL, Koibuchi N, Marino S, Martinez S, Millen KJ, Millner TO, Miyata T, Parmigiani E, Schilling K, Sekerková G, Sillitoe RV, Sotelo C, Uesaka N, Wefers A, Wingate RJ, Hawkes R. Consensus Paper: Cerebellar Development. Cerebellum. 2016 Dec;15(6):789-828. Review.
- Lewis MT, Veltmaat JM. Next stop, the twilight zone: hedgehog network regulation of mammary gland development. J Mammary Gland Biol Neoplasia. 2004 Apr; 9(2):165-81. Review.
- Lewis PM, Gritli-Linde A, Smeyne R, Kottmann A, McMahon AP. *Sonic hedgehog signaling is required for expansion of granule neuron precursors and patterning of the mouse cerebellum*. Dev Biol. 2004 Jun 15;270(2):393-410.
- Lin C, Nozawa YI, Chuang PT. *The path to chemotaxis and transcription is smoothened*. Sci Signal. 2012 Aug 21; 5(238):pe35.
- Liu YC, Couzens AL, Deshwar AR, B McBroom-Cerajewski LD, Zhang X, Puviindran V, Scott IC, Gingras AC, Hui CC, Angers S. *The PPFIA1-PP2A protein complex promotes trafficking of Kif7 to the ciliary tip and Hedgehog signaling*. Sci Signal. 2014 Dec 9; 7(355):ra117.
- Liu Z, Xiang Y, Sun G. *The KCTD family of proteins: structure, function, disease relevance*. Cell Biosci. 2013 Nov 24; 3(1):45

- Mancarelli MM, Zazzeroni F, Ciccocioppo L, Capece D, Po A, Murgo S, Di Camillo R, Rinaldi C, Ferretti E, Gulino A, Alesse E. *The tumor suppressor gene KCTD11REN is regulated by Sp1 and methylation and its expression is reduced in tumors.* Mol Cancer. 2010 Jun 30; 9:172.
- Manoranjan B, Venugopal C, McFarlane N, Doble BW, Dunn SE, Scheinemann K, Singh SK. *Medulloblastoma stem cells: where development and cancer cross pathways*. Pediatr Res. 2012 Apr; 71(4 Pt 2):516-22.
- Nüsslein-Volhard C, Wieschaus E. *Mutations affecting segment number and polarity in Drosophila*. Nature. 1980 Oct 30; 287(5785):795-801
- Oliver TG, Read TA, Kessler JD, Mehmeti A, Wells JF, Huynh TT, Lin SM, Wechsler-Reya RJ. *Loss of patched and disruption of granule cell development in a pre-neoplastic stage of medulloblastoma*. Development. 2005 May;132(10):2425-39.
- Pan Y, Bai CB, Joyner AL, Wang B. *Sonic hedgehog signaling regulates Gli2 transcriptional activity by suppressing its processing and degradation*. Mol Cell Biol. 2006 May; 26(9):3365-77.
- Petrosini L, Molinari M, Dell'Anna ME. *Cerebellar contribution to spatial event processing: Morris water maze and T-maze*. Eur J Neurosci. 1996, 8 (9): 1882-1896.
- Podlasek CA, Barnett DH, Clemens JQ, Bak PM, Bushman W. *Prostate development requires Sonic hedgehog expressed by the urogenital sinus epithelium.* Dev Biol. 1999 May 1;209(1):28-39.
- Popovic D, Vucic D, Dikic I. Ubiquitination in disease pathogenesis and treatment. Nat Med. 2014 Nov; 20(11):1242-53.
- Reardon DA, Jenkins JJ, Sublett JE, Burger PC, Kun LK. *Multiple genomic alterations including N-myc amplification in a primary large cell medulloblastoma.* Pediatr Neurosurg. 2000 Apr; 32(4):187-91.
- Rimkus TK, Carpenter RL, Qasem S, Chan M, Lo HW. *Targeting the Sonic Hedgehog Signaling Pathway: Review of Smoothened and GLI Inhibitors*. Cancers (Basel). 2016 Feb 15; 8(2). pii: E22.

- Ruiz i Altaba A, Palma V, Dahmane N. *Hedgehog-Gli signalling and the growth of the brain*. Nat Rev Neurosci. 2002 Jan; 3(1):24-33.
- Ruiz i Altaba A. *Catching a Gli-mpse of Hedgehog*. Cell. 1997 Jul 25; 90(2):193-6.
- Sahin Z, Szczepny A, McLaughlin EA, Meistrich ML, Zhou W, Ustunel I, Loveland KL. Dynamic Hedgehog signalling pathway activity in germline stem cells. Andrology. 2014 Mar; 2(2):267-74.
- Schleutker J, Baffoe-Bonnie AB, Gillanders E, Kainu T, Jones MP, Freas-Lutz D, Markey C, Gildea D, Riedesel E, Albertus J, Gibbs KD Jr, Matikainen M, Koivisto PA, Tammela T, Bailey-Wilson JE, Trent JM, Kallioniemi OP. *Genome-wide scan for linkage in finnish hereditary prostate cancer (HPC) families identifies novel susceptibility loci at 11q14 and 3p25-26*. Prostate. 2003 Dec 1; 57(4):280-9.
- Schwenk J, Metz M, Zolles G, Turecek R, Fritzius T, Bildl W, Tarusawa E, Kulik A, Unger A, Ivankova K, Seddik R, Tiao JY, Rajalu M, Trojanova J, Rohde V, Gassmann M, Schulte U, Fakler B, Bettler B. *Native GABA(B) receptors are heteromultimers with a family of auxiliary subunits*. Nature. 2010 May 13; 465(7295):231-5.
- Seddik R, Jungblut SP, Silander OK, Rajalu M, Fritzius T, Besseyrias V, Jacquier V, Fakler B, Gassmann M, Bettler B. Opposite effects of KCTD subunit domains on GABA(B) receptor-mediated desensitization. J Biol Chem. 2012 Nov 16; 287(47):39869-77.
- Seto Y, Nakatani T, Masuyama N, Taya S, Kumai M, Minaki Y, Hamaguchi A, Inoue YU, Inoue T, Miyashita S, Fujiyama T, Yamada M, Chapman H, Campbell K, Magnuson MA, Wright CV, Kawaguchi Y, Ikenaka K, Takebayashi H, Ishiwata S, Ono Y, Hoshino M. *Temporal identity transition from Purkinje cell progenitors to GABAergic interneuron progenitors in the cerebellum*. Nat Commun. 2014; 5:3337.
- Skoda AM, Simovic D, Karin V, Kardum V, Vranic S, Serman L. *The role of the Hedgehog signaling pathway in cancer: A comprehensive review*. Bosn J Basic Med Sci. 2018 Feb 20; 18(1):8-20.

- Smaldone G, Pirone L, Pedone E, Marlovits T, Vitagliano L, Ciccarelli L. The BTB domains of the potassium channel tetramerization domain proteins prevalently assume pentameric states. FEBS Lett. 2016 Jun; 590(11):1663-71.
- St-Jacques B, Hammerschmidt M, McMahon AP. *Indian hedgehog signaling regulates proliferation and differentiation of chondrocytes and is essential for bone formation.* Genes Dev. 1999 Aug 15; 13(16):2072-86.
- Stankovic T, Skowronska A. *The role of ATM mutations and 11q deletions in disease progression in chronic lymphocytic leukemia*. Leuk Lymphoma. 2014 Jun; 55(6):1227-39.
- Sudarov A, Joyner AL. Cerebellum morphogenesis: the foliation pattern is orchestrated by multi-cellular anchoring centers. Neural Dev. 2007 Dec 3; 2:26.
- Szczepny A, Hime GR, Loveland KL. *Expression of hedgehog signaling components in adult mouse testis*. Dev Dyn 2006; 235: 3063 3070
- Szczepny A, Hogarth CA, Young J, Loveland KL. *Identification of Hedgehog signaling outcomes in mouse testis development using a hanging drop-culture system*. *Biol Reprod.* 2009;80(2):258-63.
- Turner TT, Bomgardner D, Jacobs JP. *Sonic hedgehog pathway genes are expressed and transcribed in the adult mouse epididymis*. J Androl. 2004 Jul-Aug;25(4):514-22.
- Turner TT, Bang HJ, Attipoe SA, Johnston DS, Tomsig JL. *Sonic hedgehog pathway inhibition alters epididymal function as assessed by the development of sperm motility*. J Androl. 2006 Mar-Apr;27(2):225-32
- Taylor MD, Northcott PA, Korshunov A, Remke M, Cho YJ, Clifford SC, Eberhart CG, Parsons DW, Rutkowski S, Gajjar A, Ellison DW, Lichter P, Gilbertson RJ, Pomeroy SL, Kool M, Pfister SM. *Molecular subgroups of medulloblastoma: the current consensus.* Acta Neuropathol. 2012 Apr; 123(4):465-72.
- Teglund S, Toftgård R. *Hedgehog beyond medulloblastoma and basal cell carcinoma*. Biochim Biophys Acta. 2010 Apr; 1805(2):181-208.

- Van den Brink GR, Bleuming SA, Hardwick JC, Schepman BL, Offerhaus GJ, Keller JJ, Nielsen C, Gaffield W, van Deventer SJ, Roberts DJ, Peppelenbosch MP. *Indian Hedgehog is an antagonist of Wnt signaling in colonic epithelial cell differentiation.* Nat Genet. 2004 Mar; 36(3):277-82.
- Vorhees CV and Williams MT. *"Morris water maze: procedures for assessing spatial and related forms of learning and memory"* Nature protocols vol. 1,2 (2006): 848-58.).
- Vortkamp A, Lee K, Lanske B, Segre GV, Kronenberg HM, Tabin CJ. *Regulation of rate of cartilage differentiation by Indian hedgehog and PTH-related protein.* Science. 1996 Aug 2; 273(5275):613-22.
- Wada H, Makabe K. *Genome duplications of early vertebrates as a possible chronicle of the evolutionary history of the neural crest*. Int J Biol Sci. 2006; 2(3):133-41.
- Wallace VA. *Purkinje-cell-derived Sonic hedgehog regulates granule neuron precursor cell proliferation in the developing mouse cerebellum.* Curr Biol. 1999 Apr 22; 9(8):445-8.
- Wang VY, Zoghbi HY. *Genetic regulation of cerebellar development.* Nat Rev Neurosci. 2001 Jul; 2(7):484-91.
- Wechsler-Reya RJ, Scott MP. *Control of neuronal precursor proliferation in the cerebellum by Sonic Hedgehog*. Neuron. 1999 Jan; 22(1):103-14.
- Wetmore C, Eberhart DE, Curran T. *Loss of p53 but not ARF accelerates medulloblastoma in mice heterozygous for patched.* Cancer Res. 2001 Jan 15; 61(2):513-6.
- Wu LF, Gao L, Hou XM, Zhang QH, Li S, Yang YF, Lin XH. *Drosophila miR-5 suppresses Hedgehog signaling by directly targeting Smoothened.* FEBS Lett. 2012 Nov 16; 586(22):4052-60.
- Wu X, Northcott PA, Croul S, Taylor MD. *Mouse models of medulloblastoma*. Chin J Cancer. 2011 Jul; 30(7):442-9.
- Yamada M, Seto Y, Taya S, Owa T, Inoue YU, Inoue T, Kawaguchi Y, Nabeshima Y, Hoshino M. *Specification of spatial identities of cerebellar neuron progenitors by ptf1a and atoh1 for proper production of GABAergic and glutamatergic neurons*. J Neurosci. 2014 Apr 2; 34(14):4786-800.

- Yang C, Chen W, Chen Y, Jiang J. *Smoothened transduces Hedgehog signal by forming a complex with Evc/Evc2*. Cell Res. 2012 Nov; 22(11):1593-604.
- Yang ZJ, Ellis T, Markant SL, Read TA, Kessler JD, Bourboulas M, Schüller U, Machold R, Fishell G, Rowitch DH, Wainwright BJ, Wechsler-Reya RJ. *Medulloblastoma can be initiated by deletion of Patched in lineage-restricted progenitors or stem cells.* Cancer Cell. 2008 Aug 12; 14(2):135-45.
- Yao HH, Whoriskey W, Capel B. *Desert Hedgehog/Patched 1 signaling specifies fetal Leydig cell fate in testis organogenesis*. Genes Dev. 2002 Jun 1; 16(11):1433-40.
- Yi J, Wu J. *Epigenetic regulation in medulloblastoma.* Mol Cell Neurosci. 2018 Mar; 87:65-76.
- Yoganathan P, Karunakaran S, Ho MM, Clee SM. *Nutritional regulation of genome-wide association obesity genes in a tissue-dependent manner*. Nutr Metab (Lond). 2012 Jul 10; 9(1):65.
- Yoo JY, Larouche M, Goldowitz D. *The expression of HDAC1 and HDAC2 during cerebellar cortical development*. Cerebellum. 2013 Aug;12(4):534-46.
- Zanin JP, Abercrombie E, Friedman WJ. *Proneurotrophin3 promotes cell cycle withdrawal of developing cerebellar granule cell progenit ors via the p75 neurotrophin receptor*. Elife. 2016 Jul 19;5. pii: e16654.
- Zhang XM, Lin E, Yang XJ. *Sonic hedgehog-mediated ventralization disrupts formation of the midbrain-hindbrain junction in the chick embryo*. Dev Neurosci. 2000; 22(3):207-16.
- Zhang Z, Yamashita H, Toyama T, Sugiura H, Ando Y, Mita K, Hamaguchi M, Hara Y, Kobayashi S, Iwase H. *Quantitation of HDAC1 mRNA expression in invasive carcinoma of the breast**. Breast Cancer Res Treat. 2005 Nov; 94(1):11-6.
- Zou SS, Li Z, Hu HL. *Desert hedgehog regulates the proliferation and differentiation of Leydig cells: an update*. Zhonghua Nan Ke Xue. 2012 Feb; 18(2):172-5.